

Response to comments by anonymous referee #1:

In the work submitted, Lei et al. presented the design, construction, calibration and validation of a nano-HTDMA apparatus, which can be used to measure hygroscopic growth of aerosol particles down to < 10 nm. The technique they developed is very important, and they also carried out calibration and validation experiments very comprehensively. The paper is also well-written, and I only have a few comments.

Response: We are grateful to referee #1 for her/his comments and suggestions to improve our manuscript. We have implemented changes based on these comments in the revised manuscript. We repeat the specific points raised by the reviewer in italic font, followed by our response. The pages numbers and lines mentioned are with respect to the Atmospheric Measurement Techniques Discussions (AMTD) version.

General comments:

(1) Compared to “sizing accuracy”, “sizing offset” may better describe the actual content of Section 3.1.1. Sections 2.2.1 and Section 3.1.1: I think both sizing accuracy (difference between actual size and the size measured using a DMA) and sizing offset (i.e. measured difference between the two DMAs) are important for H-TDMA. While sizing offset has been carefully characterized (Section 3.1.1) for particles down to a few nm, not much information has been provided for the sizing accuracy for <100 nm particles. Although experiments to determine size accuracy for <100 nm particles seem to be impossible, as discussed in Section 2.2.1, could the author estimate the sizing accuracy from a theoretical view?

Response: Good comment, and thanks. Yes, the reviewer is right, it is not possible to determine size accuracy for < 100 nm particles, and sub-20 nm PSL is even not available. Following the reviewer’s suggestion, here we try to estimate the sizing accuracy in this size range through error propagation by using differential mobility analysis (DMA) transfer function and the uncertainties of its input parameters (Duplissy et al., 2009; Wiedensohler et al., 2012). According to Knutson and Whitby (1975), sizing of DMA transfer function mainly depends on sheath flow rates and high voltage (HV) applied to the DMA as follows:

$$z_p^* = \frac{Q_{sh} \ln \frac{r_2}{r_1}}{2\pi LV} \quad (\text{R1})$$

$$z_p^* = \frac{neC_c}{3\pi\mu d_p^*} \quad (\text{R2})$$

$$d_p^* = \frac{2VLneC_c}{3\mu Q_{sh} \ln \frac{r_2}{r_1}} \quad (\text{R3})$$

where z_p^* is the central electrical mobility, Q_{sh} is the sheath flow rate, V is the applied voltage, L is the length of the classification region within the DMA, and r_1 and r_2 are the inner and outer radii of the DMA annulus, respectively. n is the number of elementary charges of particles. e is the elementary charges. C_c is the slip correction. μ is the flow viscosity. d_p^* is the mean particle mobility diameter.

According to Eq. (R3) above, we use the following error propagation formula (Eq. (R4)) (Taylor and Taylor, 1997) to calculate the uncertainties in sizing of nanoparticles. In our study, the flow accuracy of mass flow meter (TSI series 4000) is within $\pm 2\%$. The deviation of voltage applied to the nano-DMA (0-12500 V, 0-350 V) varies around the set value when test with voltage power supply (HCE 0-12500, HCE 0-350, Fug Electronic) shown in Table R1. Thence, the sizing accuracy is obtained using Eq. (R5) as shown in Table R1.

$$\delta z = \sqrt{\left(\frac{\partial z}{\partial x}\right)^2 (\delta x)^2 + \left(\frac{\partial z}{\partial y}\right)^2 (\delta y)^2} \quad (\text{R4})$$

$$\frac{\delta d}{d} = \sqrt{\left(\frac{\delta V}{V}\right)^2 + \left(\frac{\delta Q_{sh}}{Q_{sh}}\right)^2} \quad (\text{R5})$$

Table R1 (new Table S5 in revised SI). Uncertainties of nano-DMA voltage (V) and sheath flow rates (Q_{sh}), and calculated size uncertainty.

Size (nm)	Uncertainties in V and Q_{sh}	Uncertainty (Sizing accuracy)
100	2648.2 \pm 0.02592 V, 10 \pm 0.02 L/min	0.2000%
60	1063.0 \pm 0.02686 V, 10 \pm 0.02 L/min	0.2000%
20	131.1 \pm 0.01519 V, 10 \pm 0.02L/min	0.2003%
10	33.7 \pm 0.02435 V, 10 \pm 0.02 L/min	0.2127%
8	21.6 \pm 0.03725 V, 10 \pm 0.02 L/min	0.2641%
6	12.2 \pm 0.06920 V, 10 \pm 0.02 L/min	0.6014%

Related additions and changes included in the revised manuscript:

Page 13 line 299, we add: “As discussed in Sec. 2.2.1, it is difficult to verify the sizing accuracy of sub-100 nm aerosol nanoparticles using PSL nanoparticles. Duplissy et al. (2009) and Wiedensohler et al. (2012) suggested to estimate the sizing accuracy of sub-100 nm nanoparticles through DMA transfer function. The theoretical DMA transfer function (see SI. S2. Eq. (S2-S4)) was proposed by Knutson and Whitby (1975) and they noted that sizing is crucially dependent on flow rates and high voltage (HV) applied to the DMA. In our study, the flow accuracy calibrated by the mass flow meter (TSI series 4000) is within $\pm 2\%$. The variation of voltage applied to the nano-DMAs (0-12500 V, 0-350 V) around the set value were measured with voltage power supply (HCE 0-12500, HCE 0-350, Fug Electronic) and summarized in Table S5. According to the error propagation formula (see SI. S2. Eq. (S5)) (Taylor and Taylor, 1997), the calculated uncertainty in sizing of 6-100 nm nanoparticles increases as size decreases (Table S5). The estimated sizing accuracy is slightly smaller than the sizing offset of two nano-DMAs, but in principle they are still consistent with each other. This suggests that uncertainties of slip correction, DMA dimensions (inner and outer radius, length), temperature, pressure, and viscosity of air may also affect the sizing accuracy (see SI. S2. Eq. (S4), Kinney et al., 1991). Besides, Wiedensohler et al. (2012) also suggested that particle losses, the size- and material-dependent CPC counting efficiency can affect the size accuracy of DMAs.”

Related additions included in the supplementary information:

Line 156, we add:

S2. Calculation of sizing accuracy of sub-100 nanoparticles

Knutson and Whitby (1975) proposed the following theoretical differential mobility analyzer (DMA) transfer function and showed that sizing is crucially dependent on sheath flow rates and high voltage (HV) applied to the DMA.

$$z_p^* = \frac{Q_{sh} \ln \frac{r_2}{r_1}}{2\pi LV} \quad (\text{S2})$$

$$z_p^* = \frac{neC_c}{3\pi\mu d_p^*} \quad (\text{S3})$$

$$d_p^* = \frac{2VLneC_c}{3\mu Q_{sh} \ln \frac{r_2}{r_1}} \quad (\text{S4})$$

where z_p^* is the central electrical mobility, Q_{sh} is the sheath flow rate, V is the applied voltage, L is the length of the classification region within the DMA, and r_1 and r_2 are the inner and outer radii

of the DMA annulus, respectively. n is the number of elementary charges of particles. e is the elementary charges. C_c is the slip correction. μ is the flow viscosity. d_p^* is the mean particle mobility diameter.

According to Eq. (S4) above, we use the following error propagation formula ((Taylor and Taylor, 1997) to calculate the uncertainties in sizing of nanoparticles. In our study, the flow accuracy of mass flow meter (TSI series 4000) is within $\pm 2\%$. The deviation of voltage applied to the nano-DMA (0-12500 V, 0-350 V) varies around the set value when test with voltage power supply (HCE 0-12500, HCE 0-350, Fug Electronic) shown in Table S5. Thence, the uncertainties in sizing of nanoparticles are obtained based on the following Eq. (S5) as shown in Table S5.

$$\frac{\delta d}{d} = \sqrt{\left(\frac{\delta V}{V}\right)^2 + \left(\frac{\delta Q_{sh}}{Q_{sh}}\right)^2} \quad (S5)$$

(2) Line 300-305: It is interesting to find that sizing offset ($< 0.9\%$) is smallest at 8 and 10 nm, smaller than that at smaller diameter (6 nm) and at larger diameter (20 nm or larger). Is there any explanation.

Response: Thanks for the comment. Uncertainties in the sheath flow rates and nano-DMA voltages will increase as size decreases, which results in a larger size offset of 6-nm nanoparticles compared with other sizes. However, we observed that the peak diameter of number size distribution of the generated pure water is ~ 20 -30 nm (Figure R1), which is more likely due to presence of impurities in the water. This interferes the accurate measurement of 20-nm nanoparticles.

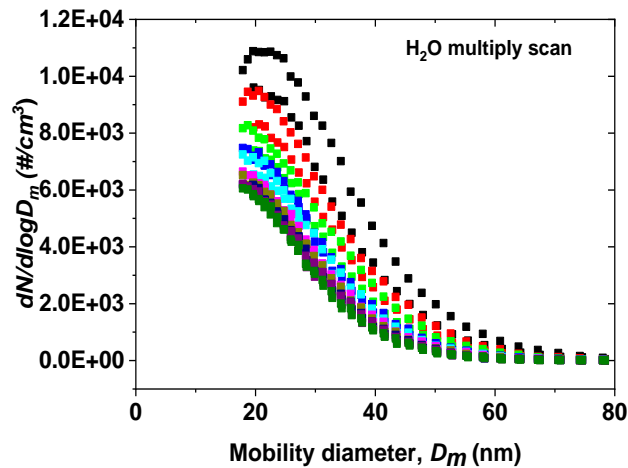


Figure R1. Number concentration scanned for water nanoparticles by the nano-DMA2 at RH below 5 % at 298 K.

Page 13 line 305, we add: “As discussed above, uncertainties in the sheath flow rates and nano-DMA voltages will increase as size decreases, which results in a larger sizing offset of 6-nm nanoparticles compared with other sizes.”

Technical comments:

(1) Line 57: change "challenge" to "challenging".

Response: Many thanks. We have revised in the following sentence and now they read as:

Page 3 line 55-57: “In addition, by knowing the hygroscopicity of newly formed nanoparticle, one can infer the involving chemical species (e.g., organic ratio) in particle formation and initial growth (Wang et al., 2010), which is otherwise difficult and highly challenging to measure directly (Wang et al., 2010; Ehn et al., 2014).”

(2) Line 349-353: I am not sure Wikipedia is a reliable source for physical/chemical constants. I would recommend textbooks/handbooks instead.

Response: Thanks for your suggestions. We have cited Atkins et al. (2006) in the following sentence:

Page 15 line 349-353: “It may due to the heat produced from the inner electrode of nano-DMA2, which we estimated to be ~ 0.08 W ($Q = mdTC_p$) by considering the density and heating capacity of air, and aerosol and sheath air flow rate ($\rho=1.2041\text{kg/m}^3$; $C_p=1.859\text{kJ/kg}^\circ\text{C}$) (Atkins et al., 2006).”

Reference:

Atkins, P., De Paula, J., and Walters, V.: Physical Chemistry, W. H. Freeman, 2006.

Kinney, P. D., Pui, D. Y. H., Mullholland, G. W. & Bryner, N. P. Use of the Electrostatic Classification Method to Size 0.1 μm SRM Particles—A Feasibility Study. *Journal of Research of the National Institute of Standards and Technology*, 96, 147, 1991.

Knutson, E. O. and Whitby, K. T.: Aerosol classification by electric mobility: apparatus, theory, and applications, *Journal of Aerosol Science*, 6, 443-451, 1975.

Taylor, J. R. and Taylor, S. L. L. J. R.: Introduction To Error Analysis: The Study of Uncertainties in Physical Measurements, University Science Books, 1997.

Wiedensohler, A., Birmili, W., Nowak, A., Sonntag, A., Weinhold, K., Merkel, M., Wehner, B., Tuch, T., Pfeifer, S., Fiebig, M., Fjåraa, A. M., Asmi, E., Sellegri, K., Depuy, R., Venzac, H., Villani, P., Laj, P., Aalto, P., Ogren, J. A., Swietlicki, E., Williams, P., Roldin, P., Quincey, P., Hüglin, C., Fierz-Schmidhauser, R., Gysel, M., Weingartner, E., Riccobono, F., Santos, S., Gruning, C., Faloon, K., Beddows, D., Harrison, R., Monahan, C., Jennings, S. G., O'Dowd, C. D., Marinoni, A., Horn, H. G., Keck, L., Jiang, J., Scheckman, J., McMurry, P. H., Deng, Z., Zhao, C. S., Moerman, M., Henzing, B., de Leeuw, G., Löschau, G., and Bastian, S.: Mobility particle size spectrometers: harmonization of technical standards and data structure to facilitate high quality long-term observations of atmospheric particle number size distributions, *Atmos. Meas. Tech.*, 5, 657-685, 2012.

Response to comments by anonymous referee #2:

This manuscript “Nano-hygroscopicity tandem differential mobility analyzer (nano-HTDMA) for investigating hygroscopic properties of sub-10 nm aerosol nanoparticles” presents a design of a HTDMA to measure the hygroscopicity particle down to ~6 nm. The performance and the methods to calibrate and validate the setup were also reported. This setup was shown to have low sizing offset (<1.4% for 100 nm particle). High accuracy for flow rates of aerosol and sheath flow ($\pm 1\%$) and high accuracy for voltages applied to DMA ($\pm 0.1\%$) were found to be crucial to achieve the low sizing offset. Also the DMA2 and humidification system were designed to be placed in housing with stable temperature ($\pm 0.1K$). The RH of sheath flow was set to the same as RH of aerosol flow to prevent the pre-deliquescence. Using this setup, the authors measured the deliquescence and the efflorescence RH as well as the growth factors of ammonium sulfate and sodium sulfate. For ammonium sulfate, no significant size dependence of DRH and ERH was observed while clear size dependence was observed. Determining the hygroscopicity of nano-particles is important to understand aerosol-water interaction and provides constraints on the chemical composition of nano-particles. This nano-HTDMA has excellent performance and will be useful to measure hygroscopicity of atmospheric nano-particles. The manuscript is well-written and fit well the scope of AMT. I recommend its publication in AMT after addressing the following minor comments.

Response: We are grateful to referee #2 for the comments and the constructive suggestions. We address in the following the comments and suggestions by referee #2 and provide improvements based on these clarify the questioned issues in the revised manuscript. The pages numbers and lines mentioned are with respect to the Atmospheric Measurement Techniques Discussions (AMTD) version.

Minor comments:

(1) What is the smallest particle size that the HTDMA can measure?

The title “Nano-hygroscopicity tandem differential mobility analyzer (nano-HTDMA) for investigating hygroscopic properties of sub-10 nm aerosol nanoparticles” reads a little redundant for me. In addition, the manuscript discusses many experiments for particle >10 nm. I suggest optimizing the title.

Response: Thanks for the comment. At the moment, the smallest size that we can measure is 6 nm. The main purpose of the instrument development is to have a device that is able to measure hygroscopic growth of sub-10 nm nanoparticles. We discussed that the results of 20 nm and 100 nm are to compare with literature studies, which are the most abundant (especially for 100 nm) and also are to demonstrate the differences between measuring hygroscopic growth of sub-10 nm nanoparticles and larger ones. Following the suggestion, we revised the title as “Nano-HTDMA for investigating hygroscopic properties of sub-10 nm aerosol nanoparticles”.

Related additions and changes included in the revised manuscript:

Page 1 line 1-2: “Nano-HTDMA for investigating hygroscopic properties of sub-10 nm aerosol nanoparticles”.

(2) Line 428-434, and Fig. 8d, the same method, electrospray was used to generate aerosol <20 nm in this study and the study by Biskos et al. 2006. But the results (growth factors) are still different. Can the authors discuss the difference? Is it possible to generate particles of the same size, i.e. 20 nm with different methods and compare the GF?

Response: Thanks for the comment.

The morphology of particles may affect their hygroscopic behavior (Mikhailov et al., 2004, 2009). Iskandar et al. (2003) and Wang et al. (2019) show that the morphology of the aerosol particles mainly depends on initial properties of droplets (e.g., chemical composition and solution concentration) and drying process. In Table 1, we compared the generation conditions with Biskos et al. 2006b for 6-10 nm ammonium sulfate nanoparticles using an electrospray. Different from generation conditions in Biskos et al. (2006b) for 6-10 nm ammonium sulfate nanoparticles, in our study, in order to minimize the multiple charged nanoparticles, three different concentrations are used so that the size (e.g., 6, 8, 10 nm) selected by the nano-DMA1 was always slight larger than peak of the number size distribution of the generated nanoparticles by the electrospray. This is to ensure that we could have as many as nanoparticles as possible to compensate the strong nanoparticle losses in the nano-HTDMA system. Besides different generation conditions shown in Table R1, the drying rate is mainly dependent on drying flow rates in the HTDMA system (Wang et al., 2019). The RH of dried ammonium sulfate aerosol nanoparticles varies due to the different aerosol/sheath flow rates employed in Biskos et al. (2006b) and this study, respectively. These

differences may lead to the small difference in growth factor of ammonium sulfate nanoparticles prior to the deliquescence.

Following reviewer’s suggestion, we used an electro spray and an atomizer to generate 20-nm ammonium sulfate aerosol nanoparticles, respectively. We then compared their hygroscopic growth factors prior to deliquescence. Figure R1a shows a ~ 0.1 higher growth factor of 20-nm ammonium sulfate generated by an electro spray than that using an atomizer in the RH range from 55% to 82%. Figure R1b shows the results of 20-nm sodium chloride nanoparticles using an electro spray and a vaporization-condensation method (Biskos et al., 2006a), respectively. Also, There is a slight difference in the growth factor of 20-nm sodium chloride at RH between 20% and 60% using the different generation methods.

Table R1. Comparison of generation of ammonium sulfate (AS) nanoparticles with diameter from 6-10 nm with Biskos et al. (2006b) using an electro spray

Generation of 6-10 nm AS nanoparticles	AS concentration (mM)	Size of capillary	Flow rates	RH of generated AS nanoparticles
Biskos et al. (2006b)	10	40 μm	2 l/min dry air	0.1%
This study	1, 5, 20	20 μm	1 l/min dry N ₂	2%

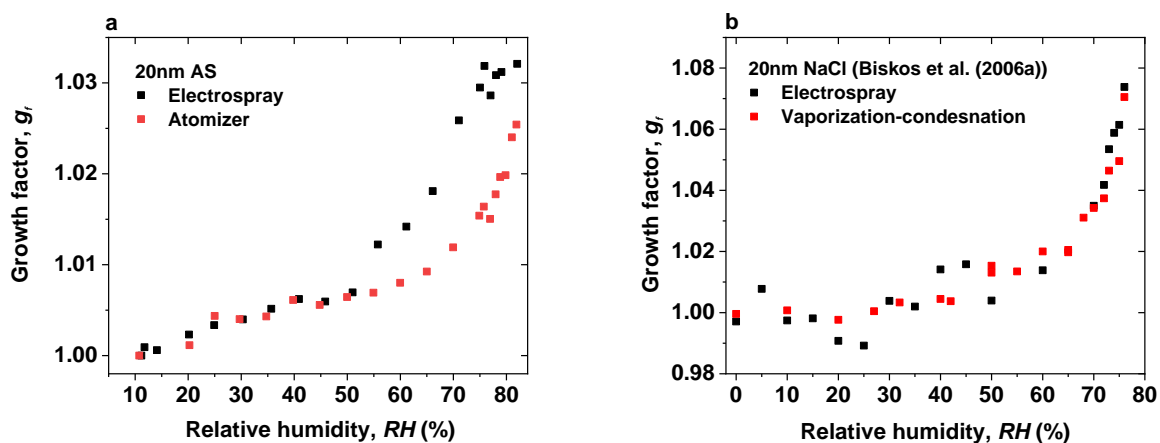


Figure R1 (new Figure S12 in revised SI). Hygroscopic growth factors of 20-nm (a) ammonium sulfate from our study (AS) nanoparticles and (b) sodium chloride (NaCl) nanoparticles from Biskos et al. (2006a) using the different generation methods prior to deliquescence.

Page 19 line 432, we add: “Different from generation conditions of for 6-10 nm ammonium sulfate nanoparticles in Biskos et al. (2006b), in our study, in order to minimize the multiple charged

nanoparticles, three different concentrations are used so that the size selected by the nano-DMA1 (i.e., 6, 8, 10 nm) was always slight larger than peak of the number size distribution of the generated nanoparticles by the electrospray. This also helps us to have as many as nanoparticles as possible to compensate the strong nanoparticle losses in the nano-HTDMA system. In addition, we used both electrospray and atomizer to generate 20-nm ammonium sulfate, and compared their hygroscopic growth factors prior to deliquescence. Figure S12a shows a ~ 0.1 higher growth factor of 20-nm ammonium sulfate generated by the electrospray than that using the atomizer in the RH range from 55% to 82%, which is similar to the difference in hygroscopic growth factor of 20-nm NaCl aerosol nanoparticles using the different generation methods as observed in Fig S12b in Biskos et al. (2006a). Besides different generation conditions, the morphology of dried ammonium sulfate particles may also differ slightly between our study and Biskos et al. (2006) because of different drying rates, as drying flow rates and RH of the dried ammonium sulfate in the two HTDMA systems are different too.”

(3) Fig. 5 and Fig. 7, can the author discuss why the 6 nm AS showed a slight increase with increasing RH.

Response: Thanks for the comments. Yes, a slight increase in hygroscopic growth factor of 6-nm ammonium sulfate nanoparticles was observed in the RH range from 65 to 79% RH before deliquesces. This is attributed to water adsorption onto the surfaces of these nanoparticles. It seems that there is more water adsorption onto the small nanoparticles than that of large nanoparticles. Similar phenomenon has also observed by Hämeri et al. (2000, 2001), Romakkaniemi et al. (2001), Biskos et al. (2006a, b, 2007), and Giamarelou et al. (2018). The reason for such enhanced adsorption at smaller sizes is still to be investigated.

Page 19 line 428, we added: “For example, a slight increase in hygroscopic growth factor of 6-nm ammonium sulfate nanoparticles is observed in the RH range from 65 to 79% RH before deliquescence. This is attributed to water adsorption onto the surfaces of these nanoparticles. It seems that smaller nanoparticles have a stronger tendency of adsorbing water when approaching the DRH than the larger ones. Similar phenomenon has also observed by Hämeri et al. (2000, 2001), Romakkaniemi et al. (2001), Biskos et al. (2006a, b, 2007), and Giamarelou et al. (2018). The reason for such enhanced adsorption at smaller sizes is still to be investigated.”

(4) Fig.7, why the DRH for 20 nm AS is different from others (the dashed line)? Also the coloring of efflorescence and deliquescence in this panel contradicts the caption.

Response: Thanks for the comment. The DRH of 20-nm ammonium sulfate is slightly different from that at other sizes. Also, the similar phenomenon was observed for 20-nm ammonium sulfate nanoparticles from Biskos et al. (2006b) shown in Fig. R2, which shows in agreement with our study. To my knowledge, we observed that the peak diameter of number size distribution of pure water is ~20-30 nm (Figure S2a), which is more likely due to presence of impurities in the water. This interferes the accurate measurement of 20-nm nanoparticles.

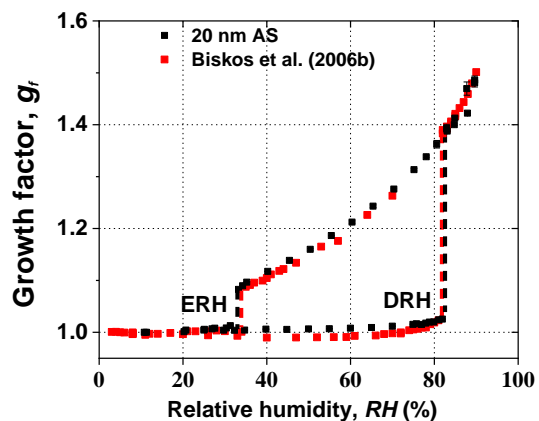


Figure R2. Comparison of the hygroscopic behavior of 20-nm ammonium sulfate (AS) with Biskos et al. (2006b).

Page 45 line 917, we revised the color of 20-nm ammonium sulfate in both deliquescence and efflorescence measurement modes and made the color consistent with citation:

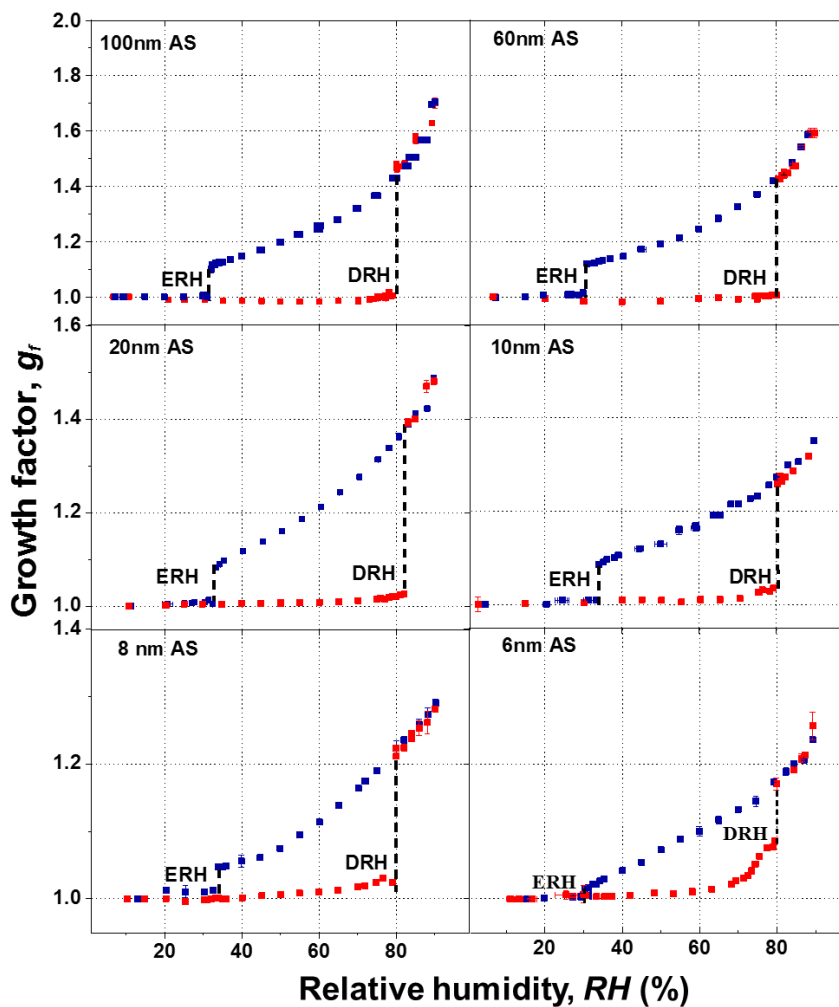


Figure 7. Mobility-diameter hygroscopic growth factors (g_f) of ammonium sulfate (AS) aerosol nanoparticles with dry mobility diameter from 6 to 100 nm in the deliquescence mode (red square and error bar) and the efflorescence mode (royal square and error bar). Deliquescence, and efflorescence relative humidity (DRH&ERH, black dashed line) of ammonium sulfate (AS) nanoparticles with dry mobility diameter from 6 to 100 nm.

(5) Line 375-376, “double-mode phenomenon was not observed 375 for 8 and 6 nm ammonium sulfate nanoparticles”. Is this because of the slower mass transfer of water vapor for larger particles?

Response: Many thanks. No, this is not because of the slower mass transfer of water vapor for larger sulfate nanoparticles. Double-mode phenomenon was observed for 99-nm sodium chloride in Mikhailov et al. (2004) and for 10-nm ammonium sulfate and sodium chloride in Biskos et al. (2006b, 2007) in the deliquescence measurement mode, respectively. They attributed this to the co-existence of solid and liquid phase of aerosol nanoparticles due to the slight inhomogeneity of RH within nano-DMA2. Bezantakos et al. (2016) have shown the difference of RH for sheath flow and aerosol flow upstream of DMA2 and temperature gradient within DMA2 can result in RH non-uniformities within DMA2. In our study, we also observed this double-mode phenomenon for ammonium sulfate nanoparticles with diameters (e.g., 100, 60, 20, 10 nm) but not for 8 and 6 nm ammonium sulfate nanoparticles. Because this phenomenon is an essentially stochastic process.

(6) Line 472-474, why does DRH/ERH of sodium sulfate show a clear size dependence while ammonium sulfate does not?

Response: Many thanks.

Different from ammonium sulfate, of which DRH and ERH shows no significant size dependence, there is a strong size-dependence of DRH and ERH of sodium sulfate according to our observations down to 6 nm. The different size dependence of DRH and ERH between sodium chloride and ammonium sulfate have been theoretically studied and explained by Cheng et al. (2015). The main reason is the different concentration dependence of solute activities and the different solute-liquid surface tension, e.g., the same change in solute molality leads to a larger change in the solute activity of sodium chloride than that of ammonium sulfate shown in Fig. R3. The phase transition concentration (deliquescence and crystallization concentration) of ammonium sulfate is thus more sensitive to the size change compared to that of sodium chloride, leading to the almost unchanged DRH and ERH of ammonium sulfate nanoparticles (Cheng et al., 2015). For the size dependence of phase transition of sodium sulfate, there is a clear size effect on DRH and ERH similar to that of sodium chloride but different from that of ammonium sulfate in the size range from 6 to 20 nm, suggesting that non-ideality of solution property is close to that of sodium chloride but weaker than that of ammonium sulfate.

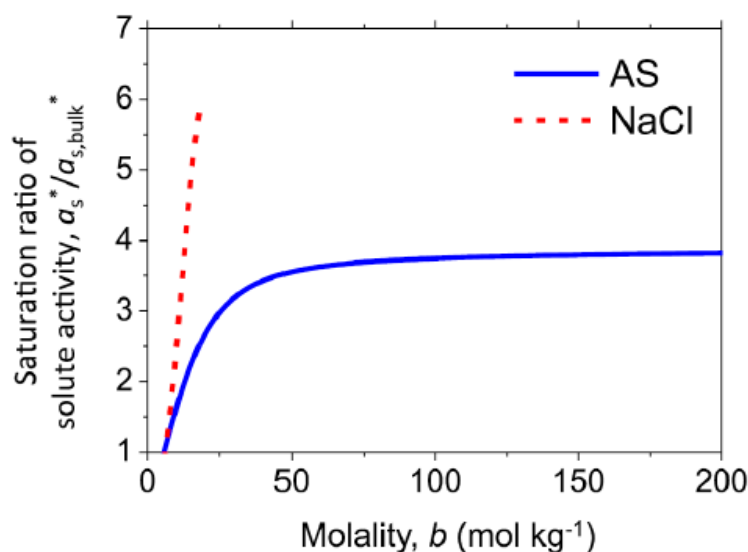


Figure R3. Saturation ratio of solute activity ($a_s^*/a_{s,bulk}^*$) as a function of molality b for ammonium sulfate (AS) and sodium chloride (NaCl). Reprinted with permission by Cheng et al. (2015).

Page 20 line 466-477, we revised: “The strong size-effect on the DRH and ERH of sodium chloride and on hygroscopic growth factors of ammonium sulfate have been observed by Biskos et al. (2006a, b, 2007) and theoretically studied and explained by Cheng et al. (2015). Owing to the strong non-ideality of aqueous ammonium sulfate solution, the phase transition concentration (deliquescence and crystallization concentration) of ammonium sulfate is much more sensitivity to the size changes from 60 nm to 6 nm than that of sodium chloride, leading to the almost unchanged DRH and ERH of ammonium sulfate nanoparticles (Cheng et al., 2015). Compared the three compounds, the size-dependent hygroscopicity of sodium sulfate nanoparticles from 20 nm to 6 nm is similar to that of sodium chloride, but different to that of ammonium sulfate, where no significant change in DRH and ERH was observed. However, in this size range, the increase of the ERH and the decrease of growth factor upon decreasing size seems to be stronger for sodium sulfate than sodium chloride, although no significant change in DRH was observed from micrometer size particles down to 20 nm.” as

“Different from ammonium sulfate, of which DRH and ERH shows no significant size dependence, there is a strong size-dependence of DRH and ERH of sodium sulfate according to our observations down to 6 nm. The different size dependence of DRH and ERH between sodium chloride and ammonium sulfate have been theoretically studied and explained by Cheng et al. (2015). The main reason is the different concentration dependence of solute activities and the different solute-liquid

surface tension, e.g., the same change in solute molality leads to a larger change in the solute activity of sodium chloride than that of ammonium sulfate. The phase transition concentration (deliquescence and crystallization concentration) of ammonium sulfate is thus more sensitive to the size change compared to that of sodium chloride, leading to the almost unchanged DRH and ERH of ammonium sulfate nanoparticles (Cheng et al., 2015). For the size dependence of phase transition of sodium sulfate, a strong size effect on DRH and ERH is similar to that of sodium chloride but different from that of ammonium sulfate in the size range from 6 to 20 nm, suggesting that non-ideality of solution property is close to that of sodium chloride but weaker than that of ammonium sulfate.”

Technical comments:

(1). Line 347, “excuses air” or “excess air”?

Response: Many thanks. We have carefully checked and revised the whole of manuscript and supplement information, including grammar, wording, and sentence structure.

Page 15 line 347-349: “we monitored that the sheath flow temperature at the inlet of nano-DMA2 is slightly lower (less than ~ 0.2 K) than that at the outlet, i.e., the RHs at the inlet of nano-DMA2 is slightly higher ($\sim 1\%$) than the RH of the excess air at the outlet.”

(2). Line 427, “continues” should be “continuous”.

Response: Many thanks. We have revised in the following sentence and now they read as:

Page 18 line 426-428: “There seems to be continuous water adsorption and the adsorbed water layers (Romakkaniemi et al., 2001) become significantly thicker when RH closer to the DRH (i.e., $RH > 70\%$).”

(3). Line 470, “sensitivity” should be “sensitive”.

Response: Many thanks. We have revised in the following sentence and now they read as:

Page 20 line 468-472: “The phase transition concentration (deliquescence and crystallization concentration) of ammonium sulfate is thus more sensitive to the size change compared to that of sodium chloride, leading to the almost unchanged DRH and ERH of ammonium sulfate nanoparticles (Cheng et al., 2015).”

(4). Fig. 5 and 6, I suggest explaining the red and blue lines in the captions, although they were explained in the main text.

Response: Many thanks. We add explanations of the red and blue lines in the all captions in the manuscript and supplement information, respectively.

Page 44 line 907-909: “**Figure 5.** Deliquescence-mode measurements of ammonium sulfate (AS) aerosol nanoparticles with dry mobility diameter from 20-6nm. The measured (black square) and fitted (solid lines) normalized size distribution are shown for increasing RH. The red and blue lines represent the aerosol nanoparticles in the solid and liquid state, respectively. The RH history in each measurement is 5% → X%, where X is the RH value given in each panel.”

Page 45 line 912-914: “**Figure 6.** Efflorescence-mode measurements of ammonium sulfate (AS) aerosol nanoparticles with dry mobility diameter from 20-6nm. The measured (black circle) and fitted (solid lines) normalized size distribution are shown for increasing RH. The red and blue lines represent the aerosol nanoparticles in the solid and liquid state, respectively. The RH history in each measurement is 5%→97%→X%, where X is the RH value given in each panel.”

Related additions and changes included in the revised supplement information:

Line 44-47: “**Figure S4.** Deliquescence-mode (a) and efflorescence-mode (b) of 100-nm ammonium sulfate (AS) aerosol nanoparticles. The measured (black square) and fitted (solid lines) normalized size distribution are shown for increasing RH (5%→X%, where X is the RH value given in each panel) and decreasing RH (5%→97%→X%, where X is the RH value given in each panel), respectively. The red and blue lines represent the aerosol nanoparticles in the solid and liquid state, respectively.”

Line 52-55: “**Figure S5.** Deliquescence-mode (a) and efflorescence-mode (b) of 60-nm ammonium sulfate (AS) aerosol nanoparticles. The measured (black square) and fitted (solid lines) normalized size distribution are shown for increasing RH (5% →X%, where X is the RH value given in each panel) and decreasing RH (5% →97% →X%, where X is the RH value given in each panel), respectively. The red and blue lines represent the aerosol nanoparticles in the solid and liquid state, respectively.”

Line 59-62: “**Figure S6.** Deliquescence-mode (a) and efflorescence-mode (b) of 8-nm ammonium sulfate (AS) aerosol nanoparticles. The measured (black square) and fitted (solid lines, single-mode log-normal fit) normalized size

distribution are shown for increasing RH (5% → X%, where X is the RH value given in each panel) and decreasing RH (5% → 97% → X%, where X is the RH value given in each panel), respectively. The red and blue lines represent the aerosol nanoparticles in the solid and liquid state, respectively.”

Line 95-100: “**Figure S9.** Deliquescence-mode **(a)** and efflorescence-mode **(b)** of 20-nm sodium sulfate aerosol nanoparticles. The measured (black square) and fitted (solid lines) normalized size distribution are shown for increasing RH (5% → X%, where X is the RH value given in each panel) and decreasing RH (5% → 97% → X%, where X is the RH value given in each panel), respectively. Red/blue solid line is fitted by a single-mode log-normal fit. Red, blue, and black lines are fitted by a double-mode log-normal fit. The red and blue lines represent the aerosol nanoparticles in the solid and liquid state, respectively. The voltage applied to the nano-DMAs (0-12500 V) is kept within ±1% around the set value shown in the voltage meter.”

Line 104-109: “**Figure S10.** Deliquescence-mode **(a)** and efflorescence-mode **(b)** of 6-nm sodium sulfate aerosol nanoparticles. The measured (black square) and fitted (solid lines) normalized size distribution are shown for increasing RH (5% → X%, where X is the RH value given in each panel) and decreasing RH (5% → 97% → X%, where X is the RH value given in each panel), respectively. Red/blue solid line is fitted by a single-mode log-normal fit. Red, blue, and black lines are fitted by a double-mode log-normal fit. The red and blue lines represent the aerosol nanoparticles in the solid and liquid state, respectively. The voltage applied to the nano-DMAs (0-350 V) is kept within ±1% around the set value shown in the voltage meter.”

Reference

Bezantakos, S., Huang, L., Barmounis, K., Martin, S. T., and Biskos, G.: Relative humidity non-uniformities in Hygroscopic Tandem Differential Mobility Analyzer measurements, *Journal of Aerosol Science*, 101, 1-9, 2016.

Biskos, G., Malinowski, A., Russell, L. M., Buseck, P. R., and Martin, S. T.: Nanosize Effect on the Deliquescence and the Efflorescence of Sodium Chloride Particles, *Aerosol Science and Technology*, 40, 97-106, 2006a.

Biskos, G., Paulsen, D., Russell, L. M., Buseck, P. R., and Martin, S. T.: Prompt deliquescence and efflorescence of aerosol nanoparticles, *Atmospheric Chemistry and Physics*, 6, 4633-4642, 2006b.

Biskos, G., Russell, L. M., Buseck, P. R., and Martin, S. T.: Nanosize effect on the hygroscopic growth factor of aerosol particles, *Geophysical Research Letters*, 33, 2007.

Cheng, Y., Su, H., Koop, T., Mikhailov, E., and Poschl, U.: Size dependence of phase transitions in aerosol nanoparticles, *Nature communications*, 6, 5923, 2015.

Giamarelou, M., Smith, M., Papapanagiotou, E., Martin, S. T., and Biskos, G.: Hygroscopic properties of potassium-halide nanoparticles, *Aerosol Science and Technology*, 52, 536-545, 2018.

Hämeri, K., Laaksonen, A., Väkevä, M., and Suni, T.: Hygroscopic growth of ultrafine sodium chloride particles, *Journal of Geophysical Research: Atmospheres*, 106, 20749-20757, 2001.

Hämeri, K., Väkevä, M., Hansson, H.-C., and Laaksonen, A.: Hygroscopic growth of ultrafine ammonium sulfate aerosol measured using an ultrafine tandem differential mobility analyzer, *Journal of Geophysical Research: Atmospheres*, 105, 22231-22242, 2000.

Iskandar, F., Gradon, L., and Okuyama, K.: Control of the morphology of nanostructured particles prepared by the spray drying of a nanoparticle sol, *Journal of Colloid and Interface Science*, 265, 296-303, 2003.

Mikhailov, E., Vlasenko, S., Martin, S. T., Koop, T., and Poschl, U.: Amorphous and crystalline aerosol particles interacting with water vapor: conceptual framework and experimental evidence for restructuring, phase transitions and kinetic limitations, *Atmospheric Chemistry and Physics*, 9, 9491-9522, 2009.

Mikhailov, E., Vlasenko, S., Niessner, R., and Poschl, U.: Interaction of aerosol particles composed of protein and salts with water vapor: hygroscopic growth and microstructural rearrangement, *Atmospheric Chemistry and Physics*, 4, 323-350, 2004.

Romakkaniemi, S., Hämeri, K., Väkevä, M., and Laaksonen, A.: Adsorption of Water on 8–15 nm NaCl and (NH₄)₂SO₄ Aerosols Measured Using an Ultrafine Tandem Differential Mobility Analyzer, *The Journal of Physical Chemistry A*, 105, 8183-8188, 2001.

Wang, X., Ma, N., Lei, T., Größ, J., Li, G., Liu, F., Meusel, H., Mikhailov, E., Wiedensohler, A., and Su, H.: Effective density and hygroscopicity of protein particles generated with spray-drying process, *Journal of Aerosol Science*, 137, 105441, 2019.

1 Nano-HTDMA for investigating hygroscopic properties of sub-10 nm aerosol 2 nanoparticles

Deleted: Nano-hygroscopicity tandem differential mobility analyzer (nano-HTDMA)

3 Ting Lei^{1,2}, Nan Ma^{4,1,3}, Juan Hong^{4,1}, Thomas Tuch³, Xin Wang², Zhibin Wang⁵, Mira Pöhlker², Maofa
4 Ge⁶, Weigang Wang⁶, Eugene Mikhailov⁷, Thorsten Hoffmann⁸, Ulrich Pöschl², Hang Su², Alfred
5 Wiedensohler³, Yafang Cheng¹

6 ¹Minerva Research Group, Max Planck Institute for Chemistry, 55128 Mainz, Germany

7 ²Multiphase Chemistry Department, Max Planck Institute for Chemistry, 55128 Mainz, Germany

8 ³Leibniz Institute for Tropospheric Research, 04318 Leipzig, Germany

9 ⁴Institute for Environmental and Climate Research, Jinan University, 511443 Guangzhou, China

10 ⁵Research Center for Air Pollution and Health, College of Environmental and Resource Science, Zhejiang University, Hangzhou,
11 310058, China

12 ⁶Beijing National Laboratory for Molecular Sciences (BNLMS), Institute of Chemistry, Chinese Academy of Sciences, Beijing,
13 100190, P. R. China

14 ⁷St. Petersburg State University, 7/9 Universitetskaya nab., St. Petersburg, 199034, Russia

15 ⁸Institute of Inorganic Chemistry and Analytical Chemistry, Johannes Gutenberg University Mainz, Mainz, Germany

16
17 *Correspondence to:* Yafang Cheng (yafang.cheng@mpic.de) and Juan Hong (juanhong0108@jnu.edu.cn)

18
19 **Abstract.** Interactions between water and nanoparticles are relevant for atmospheric multiphase processes,
20 physical chemistry, and materials science. Current knowledge of the hygroscopic and related physico-
21 chemical properties of nanoparticles, however, is restricted by limitations of the available measurement
22 techniques. Here, we present the design and performance of a nano-hygroscopicity tandem differential
23 mobility analyzer (nano-HTDMA) apparatus that enables high accuracy and precision in hygroscopic
24 growth measurements of aerosol nanoparticles with diameters less than 10 nm. Detailed methods of
25 calibration and validation are provided. Beside maintaining accurate and stable sheath/aerosol flow rates
26 ($\pm 1\%$), high accuracy of DMA voltage ($\pm 0.1\%$) in the range of ~ 0 -50 V is crucial to achieve accurate sizing
27 and small sizing offsets between the two DMAs ($< 1.4\%$). To maintain a stable relative humidity (RH), the

30 humidification system and the second DMA are placed in a well-insulated and air conditioner housing
31 (± 0.1 K). We also tested and discussed different ways of preventing pre-deliqescence in the second DMA.
32 Our measurement results for ammonium sulfate nanoparticles are in good agreement with Biskos et al.
33 (2006b), with no significant size-effect on the deliquescence and efflorescence relative humidity (DRH,
34 ERH) at diameters down to 6 nm. For sodium sulfate nanoparticles, however, we find a pronounced size-
35 dependence of DRH and ERH between 20 and 6 nm nanoparticles.

36

37 **1 Introduction**

38 The climatic effects of aerosol nanoparticles have attracted increasing interests in recent years (Wang et
39 al., 2016; Andreae et al., 2018; Fan et al., 2018), Interactions between water and nanoparticles are relevant
40 for atmospheric multiphase processes, physical chemistry, and materials science (Zheng et al., 2015; Cheng
41 et al., 2015, 2016). Aerosol nanoparticles in the atmosphere are mostly originating from new particle
42 formation, and a fraction of these nanoparticles could potentially grow into sizes to efficiently act as cloud
43 condensation nuclei and thus to change the contributions of aerosol nanoparticles to climate forcing
44 (Lihavainen 2003; Wiedensohler et al., 2009; Sihto et al., 2011; Kirkby et al., 2011; Keskinen et al., 2013;
45 Dunne et al., 2016; Kim et al., 2016). These processes strongly depend on the chemical composition and
46 physico-chemical properties of these nanoparticles (Köhler, 1936; Su et al., 2010; Wang et al., 2015; Cheng
47 et al., 2015). One of the most important physico-chemical properties of nanoparticles is their hygroscopic
48 behavior that describes their ability to take up water, and it can differ significantly from that of larger
49 particles (Hämeri et al., 2000, 2001; Gao et al., 2006; Biskos et al., 2006a, b, 2007; Cheng et al., 2015).

50 To understand and predict hygroscopic properties of nanoparticles, current thermodynamic models mostly
51 rely on the concentration-dependent thermodynamic properties (such as water activity and interfacial
52 energy) derived from the measurements of large aerosol particles or even bulk samples (Tang and
53 Munkelwitz, 1994; Tang 1996; Pruppacher and Klett, 1997; Clegg et al., 1998). They are thus difficult or

Formatted: Font color: Text 1

54 impossible to be applied to describe the hygroscopic behavior of sub-10 nm nanoparticles which can be
55 often supersaturated in concentration compared to bulk solutions (Cheng et al., 2015). Furthermore, the
56 nanosize effect on these properties may also need to be considered (Cheng et al., 2015). The lack of such
57 data hinders the understanding and an accurate simulation of the interaction of water vapor and atmospheric
58 nanoparticles. In addition, by knowing the hygroscopicity of newly formed nanoparticle, one can infer the
59 involving chemical species (e.g., organic ratio) in particle formation and initial growth (Wang et al., 2010),
60 which is otherwise difficult and highly challenging to measure directly (Wang et al., 2010; Ehn et al., 2014).
61 Hence, to measure the hygroscopicity of nanoparticles is essential to improve our understandings of aerosol
62 formation, transformation, and their climate effects.

Deleted: e

63 Different techniques have been employed to characterize the hygroscopic properties of aerosol particles in
64 different sizes (Fig. S1) (Tang et al., 2019), such as Fourier transform infrared spectrometer (FT-IR) (Zhao
65 et al., 2006), Raman spectroscopy (Dong et al, 2009), electrodynamic balance (EDB) (Chan and Chan,
66 2003, 2005; Chan et al., 2008), optical tweezers (Reid et al., 2011; Rickards et al., 2013), hygroscopicity
67 tandem differential mobility analyzer (HTDMA) (e.g., Rader and McMurry, 1986; Mikhailov et al., 2004;
68 2008; 2009; Biskos et al., 2006a, b, 2007; Cheng et al., 2008, 2009; Eichler et al., 2008; Stock et al., 2011;
69 Hong et al., 2014, 2015; Lei et al., 2014; 2018; Mikhailov and Vlasenko, 2019), and atomic force
70 microscopy (AFM) (Estillore et al., 2017). Using these techniques, most of the early lab studies focus on
71 the hygroscopic behavior of particles in accumulation modes and super-micron size range, including
72 deliquescence, efflorescence of pure components and the effect of organics on the change or suppression
73 of deliquescence and efflorescence of these inorganic components in mixtures.

Deleted: es

74 For nanoparticles with diameters down to sub-10 nm, there are, however, only very few studies attempting
75 to investigate their interactions with water molecules, which mainly utilized the setup with humidified
76 tandem DMAs (Hämeri et al., 2000, 2001; Sakurai et al., 2005; Biskos et al., 2006a, b, 2007; Giamarelou
77 et al., 2018). In Table S1, we summarized the measured DRH and ERH of ammonium sulfate nanoparticles

80 in the size range from 6 to 100 nm using HTDMAs. In these studies, the results of the observed
81 deliquescence and efflorescence relative humidity (respective DRH and ERH) and prompt or non-prompt
82 phase transitions of ammonium sulfate nanoparticles, however, do not show universal agreement. The
83 technical challenges in HTDMA measurements, especially in the sub-10 nm size range, mainly lie on: (1)
84 accurate sizing and small sizing offset of the two DMAs, (2) highly stable measurement conditions in the
85 whole system. Large sizing offset between the two DMAs may lead to significant error in the measured
86 growth factor based on error propagation (Mochida and Kawamura, 2004). Massling et al. (2011) and
87 Zhang et al. (2016) suggested that to achieve good hygroscopic growth factor of nanoparticles, the sizing
88 offset of the two DMAs should be within $\pm 2-3\%$, which is however very difficult to maintain for the sub-
89 10 nm size range. To accurately measure phase transition (e.g., DRH and ERH), a highly stable
90 measurement condition is essential, especially maintaining a small temperature perturbation in the
91 humidification system and inside the second DMA to prevent pre-deliqescence. For example, a 0.8 K
92 fluctuation of the experimental temperature during the measurement can result in a 4% difference in RH
93 (0-90%) inside the humidified DMA (Hämeri et al., 2000), leading to an inaccurate determination of the
94 phase transition. Another problem is the prompt versus non-prompt phase transition. Although effects of
95 impurities on the phase transition of aerosol nanoparticles (Biskos et al., 2006a; Russell and Ming, 2002)
96 may be one possible reason of the previously observed non-prompt phase transitions (e.g., Hämeri et al.,
97 2000), the apparent non-prompt phase transition of aerosol nanoparticles has been thought to be mainly due
98 to the inhomogeneity of RH and temperature in the humidified DMA during measurements (Biskos et al.,
99 2006b; Bezantakos et al., 2016). Moreover, the hygroscopic measurements are in general difficult for
100 nanoparticles with diameters below 20 nm due to high diffusion losses of nanoparticles (Seinfeld and
101 Pandis, 2006).

102 In this study, we present a design of nano-HTDMA setup that enables high accuracy and precision in
103 hygroscopic growth measurements of aerosol nanoparticles with diameters less than 10 nm. Detailed
104 methods of calibration and validation are provided. We discuss in detail how to maintain the good

105 performance of the system by minimizing uncertainties associated with the stability and accuracy of RH,
106 temperature, voltage for nanoparticle classification, and sheath and aerosol flows in the DMA systems. We
107 then apply the nano-HTDMA system to study the size dependence of the deliquescence and the
108 efflorescence of aerosol nanoparticles of two specific inorganic compounds (e.g., ammonium sulfate and
109 sodium sulfate) for sizes down to 6 nm.

110

111 **2. Methods**

112 **2.1 Nano-HTDMA system**

113 A nano-HTDMA system is built up to measure the aerosol nanoparticle hygroscopic growth factor (g),
114 especially aiming for accurate measurement of phase transition and hygroscopic growth factor for
115 nanoparticles in the sub-10 nm size range. Here, g is defined as the ratio of mobility diameters of
116 nanoparticles after humidification ($D_m(RH)$) to that at dry condition ($D_m(< 10\% RH)$) (see SI. [S1](#), Eq. (S1)).
117 As presented in Fig. 1, the nano-HTDMA composes three main components, including two nano-
118 differential mobility analyzers (nano-DMA, TROPOS Model Vienna-type short DMA; Birmili et al., 1997),
119 an ultrafine condensation particle counter (CPC, TSI Model 3776), and a humidification system. Table 1
120 shows the technical specification, where the DMA system, humidification system, and temperature system
121 of the three HTDMAs setup are compared among the systems of Biskos et al. (2006b), Hämeri et al. (2000)
122 and this study.

123 In our setup (Fig. 1), the first nano-DMA (nano-DMA1) is used to produce quasi-monodisperse
124 nanoparticles at a desired dry diameter. The flow rate of the closed-loop sheath flow in the nano-DMA1 is
125 maintained at 10 l/min. The ratio of sheath flow to aerosol flow is 10:1.5. The sheath flow is dried to RH
126 below 10% by two custom-built Nafion dryers (TROPOS Model ND.070) in parallel. The quasi-
127 monodisperse nanoparticles produced by nano-DMA1 then enter the humidification system, which can be

128 set to deliquescence mode (from low RH to high RH for measuring deliquescence) or efflorescence mode
129 (from high RH to low RH for measuring efflorescence). In the deliquescence mode, dry nanoparticles are
130 humidified by a Nafion humidifier (NH-1, TROPOS Model ND.070, L. 24") to a target RH. In the
131 efflorescence mode, nanoparticles are first exposed to a high RH condition (~97% RH) in a Nafion
132 humidifier (NH-2, Perma Pure Model MH-110, L. 12") and then dried to a target RH through NH-1. The
133 humid flow in the outer tube of NH-1 is a mixture of high-humidity air produced with a custom-built Gore-
134 Tex humidifier and heater (GTHH: TROPOS Model Di. 0.6", L. 11.8") and dry air in variable proportions.
135 To have a precise control of the aerosol RH, the flow rates of the humid and dry air are adjusted with a
136 proportional-integral-derivative (PID) system, including two mass flow controllers (MFC: MKS Model
137 MF1) and a RH sensor (Vaisala Model HMT330) downstream of NH-1.

138 The residence time is ~5.4 s in the NH-1 for both the deliquescence and the efflorescence modes. Many
139 groups have reported that the residence time of a few seconds is sufficient to reach equilibrium for
140 measuring hygroscopic growth or shrink of inorganic salt particles, e.g., ammonium sulfate and chloride
141 sodium (Chan and Chan, 2005; Duplissy et al., 2009; Lei et al., 2014, 2018; Giamarelou et al., 2018). More
142 specifically, Kerminen (1997) estimated the time for reaching the water equilibrium to be between 8×10^{-6}
143 s and 0.005 s for 100 nm nanoparticles at 90% RH at 25°C with accommodation coefficients from 0.001
144 to 1, respectively. In our study, we measured the inorganic aerosol nanoparticles with diameters from ~100
145 nm down to 6 nm, thus the equilibrium time should be even shorter as nanoparticle size decreases (Table.
146 S2). In NH-2, the residence time is ~0.07 s for the deliquescence of inorganic aerosol nanoparticles at very
147 high RH condition (~97% RH), which is much longer than the time estimated for phase transition by
148 Duplissy et al. (2009) (in the order of a few milliseconds) and Raoux et al. (2007) (in the order of a few
149 nanoseconds). In addition, we have tested a longer NH-2 (Perma Pure Model MH-110, L. 48") in the
150 efflorescence mode, and no significant difference in measured growth factors are found, indicating that the
151 residence time in NH-1 and NH-2 should be sufficient.

Deleted: s

153 The number size distribution of the humidified nanoparticles is measured with a combination of the second
154 nano-DMA (nano-DMA2) and the ultrafine CPC. Similar to Biskos et al. (2016b), a multiple Nafion
155 humidifier (NH-3, Pure Model PD-100) is used in our nano-HTDMA system to rapidly adjust the RH of
156 the sheath flow of nano-DMA2. The sheath flow is fed into the outer tube of NH-3 to minimize its pressure
157 drop. The RH of humid flow in the inner tube of NH-3 is controlled with a similar PID system as that for
158 NH-1. A RH sensor (Vaisala Model HMT330) downstream of NH-3 is used to provide feedback to the PID
159 system. In our nano-HTDMA system, a dew point mirror (DPM: EDGE TECH Model MIRROR-99) is
160 placed in the excess flow line to measure the RH and temperature of excess flow of the nano-DMA2. During
161 the operation, the difference between sheath flow RH and aerosol flow RH has been maintained within
162 $\pm 1\%$ (see more details in Section 2.2).

163 The sheath flow is maintained to the set flow rate with a PID-controlled recirculation blower (RB:
164 AMETEK Series MINISPIRAL). Prior to every size scan, the sheath flow rate of nano-DMA2 is adjusted
165 by the PID system according to the measurement of a mass flow meter (MFM: TSI Series 4000) in the
166 sheath flow line. In order to minimize the pressure drop along the recirculating sheath flow loop, low flow
167 resistance MFM and hydrophobic filter (HF: Whatman Model 6702-3600) are used. A heat exchanger (HE,
168 Ebmpapst Model 4414FM) is installed downstream of the RB to minimize the temperature perturbation in
169 the sheath flow by the heat generated in the RB.

170 As aforementioned, temperature non-uniformity is the main contributor to the fluctuation of RH within
171 humidified DMA. Temperature difference within nano-DMA2 is unavoidable mainly due to temperature
172 difference between inner electrode and the rest of nano-DMA2 parts and/or the temperature difference
173 between aerosol and sheath flow (Duplissy et al., 2009; Bezantakos et al., 2016). As shown in Fig. 1, to
174 investigate and monitor the temperature difference within nano-DMA2 during measurements, a
175 temperature sensor (THERMO ELECTRON Model Pt100) is placed at the inlet of the sheath flow and the
176 temperature of sheath excess flow is monitored by the DPM. Note that, a DPM should be installed as close

177 as possible to the nano-DMA2 in the excess flow, which better represents the conditions inside the nano-
178 DMA2, such as temperature and RH (Wiedensohler et al., 2012). In addition, the temperature of aerosol
179 flow is monitored at the inlet of the aerosol flow of nano-DMA2.

180 Moreover, to maintain a stable environment that required for the growth factor measurements, nano-DMA2
181 with its sheath flow humidification system is placed in a well-insulated housing chamber (marked with
182 yellow dashed lines in Fig. 1). An air conditioner (Telemeter Electro Model TEK-1004-RR-24-IP55) is
183 installed inside the housing to maintain a constant temperature (292.15 ± 0.1 K), which is set to be ~ 1 K
184 lower than the constant laboratory temperature (293 K) in order to achieve high RH ($\sim 90\%$) inside nano-
185 DMA2.

186 **2.2 Calibration of nano-HTDMA**

187 The purpose of this study is to design and build a nano-HTDMA system that is able to measure the
188 hygroscopic properties of nanoparticles, especially in the sub-10 nm size range. A small perturbation in the
189 measurement conditions may lead to large biases in the results. Hence, to provide high quality
190 hygroscopicity measurements of nanoparticles, systematic calibration of the nano-HTDMA should be
191 conducted regularly to ensure the accuracy and stability of the measurement conditions. Table 1 lists the
192 possible sources of uncertainty, which could affect the performance of the HTDMAs. In our setup,
193 nanoparticle sizing, aerosol/sheath flow rates, the high voltage (HV) applied to nano-DMAs, RH sensors,
194 and temperature sensors are calibrated and verified independently.

195 Note that in the following, for calibration and/or checking of different parameters, the criteria and/or
196 standard that the nano-HTDMA system has to meet are listed mainly according to the suggestions from
197 Duplissy et al., (2009) and Wiedensohler et al. (2012), which are not specifically provided for accurately
198 measuring sizes or hygroscopic growth of sub-10 nm nanoparticles. Compared with these criteria, to
199 measure hygroscopic growth of sub-10 nm nanoparticles, we have achieved a better condition for our nano-

200 HTDMA system after comprehensive calibrations described as follows (more details about performance of
201 our system see section 3).

202 **2.2.1 Sizing accuracy**

203 For particle diameters higher than 100 nm, the verification of sizing accuracy of DMAs can be
204 accomplished by using certified particles of known sizes such as polystyrene latex (PSL) spheres (Hennig
205 et al., 2005; Mulholland et al., 2006; Duplissy et al., 2009; Wiedensohler et al., 2012, 2018). The particle
206 sizing of nano-DMA2 is checked with PSL by switching off the sheath flow and the HV supply of nano-
207 DMA1, which actually in this case does not function as a DMA, but rather a stainless-steel tube. Sizing
208 agreement between measured diameters and nominal diameters of PSL particles above 100 nm should be
209 within $\pm 3\%$ (Wiedensohler et al., 2012). After confirming the accurate sizing of nano-DMA2, the sizing
210 accuracy of nano-DMA1 can be in turn checked by the nano-DMA2 with a full scan of a certain size of
211 PSL selected by the nano-DMA1. Note that, it is important to check not only the sizing accuracy of both
212 DMAs, but also the sizing agreement between the nano-DMA1 and nano-DMA2. To achieve good
213 hygroscopicity measurements of nanoparticles, the sizing offset of the two DMAs should be within $\pm 2-3\%$
214 (Massling et al., 2011; Zhang et al., 2016).

215 For nanoparticles with diameters smaller than 100 nm, the sizing accuracy is, however, difficult to check
216 by using PSL nanoparticles. This is mainly because the size of residual material in the solution also peaks
217 around 20 – 30 nm (Fig. S2a), resulting in an asymmetric number size distribution of generated PSL
218 nanoparticles (Fig. S2b) (Wiedensohler et al., 2012). PSL nanoparticles with diameters below 20 nm are
219 not commercially available (<https://www.thermofisher.com/order/catalog/product/3020A>), making the
220 verification in this size range even impossible. Sizing accuracy of nanoparticles is critically determined by
221 sheath flow rates and HV applied to the nano-DMAs. However, unlike for the 100 nm nanoparticles, a $\pm 2-$
222 3% sizing offset between the two DMAs would be very difficult to maintain for nanoparticles with
223 diameters smaller than 20 nm. Thence, accurate calibrations of sheath flow rates and high voltage are crucial

224 for constraining the uncertainty associated with sizing of nanoparticles below 100 nm. The calibrations for
225 aerosol/sheath flow, DMA voltage, and sensors will be described in detail in the following Section 2.2.2-
226 2.2.5.

227 **2.2.2 Aerosol and sheath flow**

228 Sizing accuracy of a DMA directly depends on the accuracies of aerosol and sheath flow rates. The aerosol
229 flow rate at the inlet of the nano-DMA1 is checked by using a bubble flow meter (Gilian Model Gilibrator-
230 2). Wiedensohler et al. (2012) recommended that the measured aerosol flow rate should not deviate more
231 than 5% from the set flow rate during the measurements, otherwise one should check the flow rate of CPC
232 or if there is a leakage in the system. Details about leakage checking can be found in Birmili et al. (2016).

233 To calibrate the sheath flow, a verified MFM (TSI Series 4000) is placed in the recirculating sheath flow
234 close-loop upstream of the MFM. By applying a series of sheath flow rates, a calibration curve (flow rate
235 vs. MFM analogue output) can be obtained according to the reading of the reference MFM. Maximum
236 deviation of 2% from the sheath flow rate value of the reference MFM is recommended by Wiedensohler
237 et al. (2012), which can keep sizing accuracy of 200 nm PSL particles within $\pm 2\%$.

238 **2.2.3 DMA voltage**

239 The sizing of nano-DMAs is very sensitive to the accuracy and precision of the voltages applied, especially
240 when measuring nanoparticles in the sub-10 nm diameter range. A verified reference voltage meter with
241 voltage up to 1000 V (Prema Model 5000 DMM, accuracy 0.005%) is used to calibrate the HV supply of
242 the nano-DMAs (0-350 V). By setting a series of analogue voltage values, the HV applied to nano-DMA
243 can be calibrated according to the values shown in the reference voltage meter. For our nano-DMAs, sub-
244 10 nm in particle sizes correspond to voltage below 50 V. Thence, voltage calibration should be performed
245 with a higher resolution (smaller voltage interval) from 0 to 50 V (shown in the insert of Fig. 2).

246 **2.2.4 RH sensor**

247 One typical method to calibrate RH sensors in a HTDMA system is to measure the hygroscopic growth
248 factors of ammonium sulfate (Hennig et al., 2005), although the effects of shape factors, restructuring, and
249 impurities in the solutions may hamper a reliable RH calibration with this method (Duplissy et al., 2009).
250 Moreover, this indirect RH sensor calibration through measurement of the hygroscopic growth factors of
251 ammonium sulfate (usually with nanoparticle diameters around or above 100 nm) only calibrates the RH
252 values higher than the ERH of the pure salt. Calibration of RHs below ERH of ammonium sulfate is
253 important for the phase transition measurements. Most importantly, we are investigating the hygroscopic
254 growth factors of ammonium sulfate nanoparticles. Hence, using ammonium sulfate nanoparticles to
255 calibrate RH sensors in our system becomes invalid.

Deleted:

256 Therefore, we alternatively calibrate the RH sensors by using a DPM (EDGE TECH Model MIRROR-99),
257 which is recommended in several previous studies (Hennig et al., 2005; Duplissy et al., 2009; Biskos et al.,
258 2006a, b, 2007). In the calibration, the DPM and RH sensors should be kept in the well-insulated chamber
259 with constant laboratory conditions (e.g., flow rates, temperature, and pressure). By running the DPM and
260 all the other RH sensors in parallel at various RHs (5% to 90%), a calibration curve of the RHs measured
261 by the DPM against analogue voltages of RH sensor can be obtained.

262 **2.2.5 Temperature sensor**

263 Since all our temperature sensors and the high accurate DPM (EDGE TECH Model MIRROR-99) are
264 installed in the aforementioned well-insulated chamber and the chamber temperature is maintained with air
265 conditioner at about 292.15 ± 0.1 K, we calibrate the temperature sensors and corrected their systematic shift
266 by comparing the record of temperature sensors and the DPM by keeping them in parallel inside the
267 chamber over a 12-hour time period.

268 **2.3 Particle generation**

270 The experiments shown in this study were conducted using laboratory generated ammonium sulfate and
271 sodium sulfate nanoparticles. Nanoparticles with diameters of 6, 8, and 10 nm were generated by an
272 electrospray (AG: TSI Model 3480) with 1, 5, and 20 mM aqueous solution of ammonium sulfate and
273 sodium sulfate (Aldrich, 99.99%), respectively. The generated particles were then diluted and dried to RH
274 below 2% by mixing with dry and filtered N₂ (1 l/min) and CO₂ (0.1 l/min). The dried polydisperse aerosol
275 nanoparticles were subsequently neutralized by a Po²¹⁰ neutralizer. To avoid blocking the 25- μ m capillary
276 of the electrospray with high solution concentration, we used an atomizer (AG: TSI Model 3076) to
277 generate nanoparticles with diameters of 60-100 nm and 20 nm with 0.05 and 0.001 wt% solution of
278 ammonium sulfate and sodium sulfate (Aldrich, 99.99%), respectively. Also, 100-nm PSL nanoparticles
279 were atomizing a PSL solution of mixing 3 drops of 100-nm PSL with 300 mL distilled and de-ionized
280 milli-Q water. The generated nanoparticles were subsequently dried to RH below 10% with a custom-built
281 Nafion dryer (ND: TROPOS Model ND.070) and then neutralized by a Kr⁸⁵ neutralizer.

282 The solutions used in our measurements were prepared with distilled and de-ionized milli-Q water
283 (resistivity of 18.2 M Ω cm at 298.15 K). Note that, for 100-60 nm and 20 nm, the solution concentration
284 was adjusted so that the sizes selected by the nano-DMA1 were always larger than the peak diameter of the
285 number size distribution of the generated nanoparticles to minimize the influence of the multiple charged
286 nanoparticles in hygroscopicity measurements. The influence of multiple charges on sub-10 nm particles
287 is expected to be very small, we, however, still used different concentrations so that the sizes selected by
288 the nano-DMA1 were always around the peak of the number size distribution of the generated nanoparticles
289 by the electrospray (Fig. S3). This is to ensure that we could have as many particles as possible to
290 compensate the strong loss of very small particles in the whole humidification systems.

291

292 **3 Results and discussion**

293 **3.1 Performance of the nano-HTDMA**

294 **3.1.1 Sizing accuracy**

295 In this section, we show the performance of our nano-HTDMA after a full calibration, including accuracy
296 and stability of the aerosol/sheath flow rates, the voltage applied to the nano-DMA, and nanoparticle-
297 sizing accuracy. In our study, the sheath/aerosol flow rates and nano-DMA voltage supply have been
298 calibrated every day and every two weeks, respectively. The deviations of the measured aerosol/sheath flow
299 rates from the set-point values are less than $\pm 1\%$, which is lower than the maximum variation of 2%
300 recommended by Wiedensohler et al. (2012).

301 The voltage applied to the nano-DMA (up to 350 V) is kept within $\pm 0.1\%$ around the set value shown in
302 the voltage meter. As shown in Fig. 3a, when test with 100-nm PSL nanoparticles, the average peak
303 diameter of scans from the nano-DMA2 is 100.4 nm, which matches well with the mean diameter of PSL
304 nanoparticles (100 ± 3 nm, Thermo Fisher Scientific Inc.). Afterwards, when using nano-DMA1 select 100
305 nm PSL, the scanned size distribution by nano-DMA2 has a peak diameter at 100.3 nm (Fig. 3b), indicating
306 a good sizing accuracy of the nano-DMA1 too. As discussed in Sec. 2.2.1, it is difficult to verify the sizing
307 accuracy of sub-100 nm aerosol nanoparticles using PSL nanoparticles. Duplissy et al. (2009) and
308 Wiedensohler et al. (2012) suggested to estimate the sizing accuracy of sub-100 nm nanoparticles through
309 DMA transfer function. The theoretical DMA transfer function (see SI. S2. Eq. (S2-S4)) was proposed by
310 Knutson and Whitby (1975) and they noted that sizing is crucially dependent on flow rates and high voltage
311 (HV) applied to the DMA. In our study, the flow accuracy calibrated by the mass flow meter (TSI series
312 4000) is within $\pm 2\%$. The variation of voltage applied to the nano-DMA (0-12500 V, 0-350 V) around the
313 set value were measured with voltage power supply (HCE 0-12500, HCE 0-350, Fug Electronic) and
314 summarized in Table S5. According to the error propagation formula (see SI. S2. Eq. (S5)) (Taylor and
315 Taylor, 1997), the calculated uncertainty in sizing of 6-100 nm nanoparticles increases as size decreases
316 (Table S5). The estimated sizing accuracy is slightly smaller than the sizing offset of two nano-DMA, but
317 in principle they are still consistent with each other. This suggests that uncertainties of slip correction, DMA

Formatted: Font color: Text 1

318 dimensions (inner and outer radius, length), temperature, pressure, and viscosity of air may also affect the
319 sizing accuracy (see SI. S2. Eq. (S4), Kinney et al., 1991). Besides, Wiedensohler et al. (2012) also
320 suggested that particle losses, the size- and material-dependent CPC counting efficiency can affect the size
321 accuracy of DMAs,

Formatted: Font color: Red

322 After calibration, on average a <1.4% sizing offset between the two nano-DMAs can be achieved for
323 ammonium sulfate nanoparticles with dry diameters of 100 nm, 60 nm and 20 nm (Fig. 3c, Fig.5, Table S3,
324 Fig. S4, and Fig. S5), which is much better than the 2-3% criteria recommended by Massling et al. (2011)
325 and Zhang et al. (2016). For sub-10 nm ammonium sulfate nanoparticles, our system has an average sizing
326 offset of <0.9% for 10 and 8 nm particles and ~1.4% for 6 nm particles, respectively (Fig. 3d, Fig. 5, Table

327 S3, and Fig. S6). As discussed above, uncertainties in the sheath flow rates and nano-DMA voltages will
328 increase as size decreases, which results in a larger sizing offset of 6-nm nanoparticles compared with other
329 sizes. Note that, we also tested to calibrate the DMA voltage with a voltage meter with lower accuracy of
330 $\pm 1\%$, and the DMA voltages can only be kept within $\pm 1\%$ around the set value. In this way, we found a
331 much larger sizing offset for the sub-10 nm particles, i.e., 5.4% and 6.0% for 8 and 6 nm ammonium sulfate
332 nanoparticles, respectively. These results show that maintaining an accurate sheath/aerosol flow (with $\pm 1\%$
333 around the set value) together with a careful voltage calibration (with $\pm 0.1\%$ around the set value, especially
334 in low voltage range, i.e., <50 V for our system) is the key for accurate sizing of sub-10 nm nanoparticles.

Formatted: Font color: Text 1

335 **3.1.2 Preventing pre-deliqescence in the deliqescence measurement mode**

336 Pre-deliqescence of dry nanoparticles in the deliqescence measurement mode is an important issue that
337 needs to be resolved in order to obtain accurate DRH (Biskos et al., 2006b; Duplissy et al., 2009;
338 Bezantakos et al., 2016; Hämeri et al., 2000). Since temperature and RH are closely linked and accurate
339 monitoring of these two quantities in the system are critical for nano-HTDMA measurements, we calibrated
340 all RH and T sensors regularly (every two weeks in this study). To prevent pre-deliqescence and optimize
341 the system, we have conducted three tests using ammonium sulfate nanoparticles with a dry diameter of

342 100 nm. In the first test, we regulated the RH of excess flow (RH_e) and made it equal to that of the aerosol
343 flow at the inlet of nano-DMA2 (RH_a), i.e., $RH_e=RH_a$, as done by previous HTDMA measurements, e.g.,
344 Villani et al. (2008). As shown in Fig. 4a, the measured growth factors of 100-nm ammonium sulfate are
345 in good agreement with predictions of the Extended Aerosol Inorganic Model (E-AIM; Clegg et al., 1998)
346 at RH above 80%. However, the ammonium sulfate nanoparticles deliquesce at 75% RH, which is
347 significantly lower than the expected DRH (80%, Tang and Munkelwitz (1994)). Since our RH sensors
348 were all well calibrated and the uncertainty of RH measurement is $\pm 1\%$, it is reasonable to hypothesize that
349 the RH upstream of nano-DMA2 has already reached the deliquesce RH of ammonium sulfate
350 nanoparticles. When these aerosol nanoparticles move downstream of the nano-DMA2, the RH decreases
351 back to 75%, which dehydrates the deliquesced ammonium sulfate nanoparticles. To avoid the pre-
352 deliquescence, Hämeri et al. (2001) has suggested to set RH_a to be 3-5% lower than RH_e . In the second test,
353 we have configured and regulated the system following this suggestion, i.e., $RH_e \geq RH_a + 3\%$. In this case,
354 the ammonium sulfate nanoparticles still deliquesce at 79% RH (Fig. 4b), even if RH_a is 6% lower than
355 RH_e .

356 Previous studies (Biskos et al., 2006b; Bezantakos et al., 2016) have shown that RH non-uniformities within
357 the nano-DMA2 can result in inaccurate measurements of phase transition and hygroscopic growth of
358 aerosol nanoparticles. One reason for RH non-uniformities within nano-DMA2 is that the sheath flow RH
359 is different from the aerosol flow RH at the inlet of the DMA (Hämeri et al., 2000, 2001). Another important
360 reason is the existence of temperature gradient within nano-DMA2 (Bezantakos et al., 2016). Hence, in the
361 third test, we moved the RH sensor from the excess flow downstream of nano-DMA2 to the sheath flow
362 upstream of nano-DMA2 and then regulated RH of sheath flow (RH_s) the same as RH_a (shown in Fig. 1),
363 i.e., $RH_s=RH_a$, as done by Kreidenweis et al. (2005), Biskos et al. (2006a, b), and Massling et al. (2011).

364 Note that to minimize the temperature gradient within the nano-DMA2 in our system so that nanoparticles
365 can undergo almost the same RH conditions, the nano-DMA2 with its sheath flow humidification system
366 has been placed in a well-insulated air-conditioned chamber. The air temperature inside the chamber can

Deleted: .

368 be maintained at an almost constant level (292.15 ± 0.1 K). In addition, a heat exchanger was installed
369 downstream of the recirculation blower to minimize the temperature perturbation in the sheath flow by the
370 heat generated in the RB. Unlike previously reported by Bezantakos et al. (2016) that the RH at the outlet
371 was higher than that the inlet of the sheath air, we monitored that the sheath flow temperature at the inlet
372 of nano-DMA2 is slightly lower (less than ~ 0.2 K) than that at the outlet, i.e., the RH_s at the inlet of nano-
373 DMA2 is slightly higher ($\sim 1\%$) than the RH of the excess air at the outlet. It may due to the heat produced
374 from the inner electrode of nano-DMA2, which we estimated to be ~ 0.08 W ($Q = mdT C_{p,k}$) by considering
375 the density and heating capacity of air, and aerosol and sheath air flow rate ($(\rho = 1.2041 \text{ kg/m}^3; C_p =$
376 $1.859 \text{ kJ/kg}^\circ\text{C})$ (Atkins et al., 2006). Although this temperature perturbation (less than ~ 0.2 K between the
377 sheath flow at the inlet and the excess flow at the outlet of the nano-DMA2) is larger than the ideal condition
378 of less than 0.1 K that Duplissy et al. (2009) and Wiedensohler et al. (2012) suggested, our experimental
379 results show that a prompt phase transition can be still achieved. In this case, the measured DRH of
380 ammonium sulfate nanoparticles is almost at 80% (Fig. 4c and 4d).

381 3.1.3 Prompt phase transition of ammonium sulfate

382 Figure 5 and 6 show the normalized particle number size distributions measured by the nano-DMA2 in the
383 respective deliquescence and efflorescence measurement modes for ammonium sulfate nanoparticles with
384 dry mobility diameters of 20 nm, 10 nm, and 6 nm (see Fig. S4 for 100 nm, see Fig. S5 for 60 nm, see Fig.
385 S6 for 8 nm). In the deliquescence measurement mode (Fig. 5, Fig. S4a, and Fig. S5a), we observed the
386 similar double-mode phenomenon as reported by Mikhailov et al. (2004) and Biskos et al. (2006b, 2007).
387 For example, at 20 nm, there are two distinct intersecting modes of particle size distributions determined
388 by the nano-DMA2 in the RH range from 79% to 83% RH (around the DRH of ammonium sulfate). Biskos
389 et al. (2006b, 2007) attributed these two modes to the co-existence of solid and liquid phase nanoparticles
390 at RH close to the DRH of ammonium sulfate, due to the slight inhomogeneity of RH in the second nano-
391 DMA, i.e., some nanoparticles have already undergo deliquescence (liquid state) and some are not (solid).

Deleted: uses

Deleted: ; https://en.wikipedia.org/wiki/Density_of_air;
https://www.engineeringtoolbox.com/water-vapor-d_979.html

Formatted: Default Paragraph Font, Font: (Default)
+Body (Calibri), 11 pt

Formatted: Default Paragraph Font, Font: (Default)
+Body (Calibri), 11 pt

396 This is evident through a double-mode log-normal fitting (red and blue modes in Fig. 5). Until RH ~82%,
397 the peak diameter of the red mode at 82% RH is similar to that at 11% RH, indicating that these
398 nanoparticles are still in a solid state. At 82% RH, a population of ammonium sulfate nanoparticles starts
399 to deliquesce and exists in a distinct mode with significant larger peak diameter (blue mode), although
400 majority of the nanoparticles remain solid (red mode). Further increase RH, the peak diameter of
401 normalized number size distribution of the blue mode increases, indicating the continuous growth the
402 nanoparticles after deliquescence. However, in our case the double-mode phenomenon was not observed
403 for 8 and 6 nm ammonium sulfate nanoparticles (Fig. 5 and Fig. S6a). To have a better estimation of DRH
404 when the double modes occurred, the peak diameter of the mode with larger number of nanoparticles was
405 chosen for growth factor calculation (Biskos et al., 2006b, 2007). For example, for 20 nm ammonium
406 sulfate nanoparticles, the peak diameters of normalized number size distribution of the red and blue modes
407 are used to calculate growth factor at RH between 79% to 83%, respectively.

408 For the efflorescence measurement mode, we adopted the approach of Biskos et al. (2006b) and used the
409 geometric standard deviation of number size distribution (σ) to quantify the diversity of the sizes of
410 nanoparticles. As shown in Fig. 6, Fig. S4b, Fig. S5b, and Fig. S6b, broadening of the normalized number
411 size distributions measured with nano-DMA2 was only observed for 20-nm ammonium sulfate
412 nanoparticles in the RH range from 33% to 30%. There, at RH higher than 33% or lower than 30%, σ stays
413 stably at 1.072. However, clear increases of σ (1.078-1.087) were observed for RH between 33% and 30%.
414 The normalized number size distributions in the RH range from 33% to 30% can be further resolved by
415 double-mode fit with fixed σ of 1.072 (the red and the blue mode in Fig. 6 for 20 nm). The ammonium
416 sulfate nanoparticles in the red mode at RH between 33% to 30% are in solid state because the peak diameter
417 of red mode is similar as that at 11% RH. However, within this RH range, the peak diameter of the blue
418 mode is significantly larger, indicating that these nanoparticles are still in liquid state. Further decreasing
419 RH (lower than 30%), only one mode has been observed and the peak diameter of the normalized number
420 size distribution almost unchanged as RH decreases (red mode in Fig. 6 for 20nm), which means that the

Deleted:

422 nanoparticles have been all in the solid state. Similar to the deliquescence measurement shown above and
423 in Fig. 5, the co-existence of solid and aqueous phase nanoparticles at RH 30-33% is also very likely to
424 stem from the slight heterogeneous RH in nano-DMA2 (Biskos et al., 2006b). To have a better estimation
425 of ERH when the broadening phenomenon exists, the peak diameter of the mode with larger number of
426 nanoparticles was used for growth factor calculation. After such data processing in both deliquescence and
427 efflorescence modes, we obtained prompt deliquescence and efflorescence of 6 to 100 nm ammonium
428 sulfate nanoparticles (more details in Section 3.1.4).

429 **3.1.4 Size-dependent hygroscopicity of ammonium sulfate nanoparticles**

430 Figure 7 shows the humidogram of ammonium sulfate nanoparticles measured by our nano-HTDMA
431 system in the size (dry diameter) range of 6-100 nm. The detailed comparison between our results and
432 Biskos et al. (2006b) during both deliquescence and efflorescence measurements are presented in Fig. 8a
433 and b (also Fig. S7). In general, our results are in a good agreement with the measurement results of Biskos
434 et al (2006) and the theoretical prediction by Cheng et al. (2015). First, there is a strong size dependence in
435 the hygroscopic growth factor of ammonium sulfate nanoparticles, and smaller ammonium sulfate
436 nanoparticles exhibit lower growth factor at a certain RH. For example, the difference of the growth factor
437 between 6 and 100 nm nanoparticles is up to 0.28 at 80% RH (Fig. S8a). Second, there is, however, no
438 significant size dependence in both DRH and ERH (Fig. S8b). For nanoparticles of different sizes (6-100
439 nm), the DRH and ERH of ammonium sulfate varies slightly from ~80-83% and ~30-34%, respectively.
440 This variation of the DRH and ERH along the size is much smaller for ammonium sulfate nanoparticles
441 than for sodium chloride (Biskos et al. 2006a, 2007).

442 Although our results in general agree well with Biskos et al. (2006b), the growth factors of 10, 8, and 6 nm
443 ammonium sulfate nanoparticles that we measured at high RH (i.e., > ~70%) are slightly lower (~0.02 in
444 growth factor) than that in Biskos et al. (2006b) in both deliquescence and efflorescence processes (Fig. 8b
445 and Fig. S7). We calculated the uncertainties of growth factor of 10-nm ammonium sulfate from 80% to

446 90% RH for our system and Biskos et al. (2006b) system by $\sqrt{\left(\left(g_f \frac{\sqrt{2}\epsilon_{Dp}}{D_p}\right)^2 + \left(\epsilon_{RH} \frac{dg_f}{dRH}\right)^2\right)}$ (Mochida

447 and Kawamura, (2004)). Here, ϵ_{Dp} , ϵ_{RH} , and g_f are uncertainty of particle mobility diameter, uncertainty
448 of relative humidity, and growth factor with respect to RH, respectively. The average sizing offsets of our

449 system and Biskos et al. (2006b) for 10 nm ammonium sulfate are taken here as $\frac{\epsilon_{Dp}}{D_p}$ (see Table 1). As shown
450 in the insert of Fig. 8b, the discrepancies between the two systems are still within measurement uncertainty.

451 In addition, compared to Biskos et al. (2006b), our results show a similar re-structuring in deliquescence
452 mode at RH between about 20% to 75% for 100, and 60 nm ammonium sulfate nanoparticles (Fig 8c).

453 However, different than in Biskos et al. (2006b), we do not find re-structuring for smaller ammonium
454 sulfate nanoparticles (20, 10, 8, and 6 nm) at RH below deliquescence point (Fig. 8c and Fig. 8d). There

455 seems to be continuous water adsorption and the adsorbed water layers (Romakkaniemi et al., 2001)

456 become significantly thicker when RH closer to the DRH (i.e., RH > 70%). For example, a slight increase
457 in hygroscopic growth factor of 6-nm ammonium sulfate nanoparticles is observed in the RH range from

458 65 to 79% RH before deliquescence. This is attributed to water adsorption onto the surfaces of these
459 nanoparticles. It seems that smaller nanoparticles have a stronger tendency of adsorbing water when

460 approaching the DRH than the larger ones. Similar phenomenon has also observed by Hämeri et al. (2000,
461 2001), Romakkaniemi et al. (2001), Biskos et al. (2006a, b, 2007), and Giamarelou et al. (2018). The reason

462 for such enhanced adsorption at smaller sizes is still to be investigated. Note that, the ammonium sulfate
463 hygroscopic data from Biskos et al. (2006b) shown here are all generated by an electrospray, but in our

464 experiments, only the ammonium sulfate nanoparticles with diameters smaller than 20 nm (i.e., 10, 8, and
465 6 nm) were generated by an electrospray, while the larger nanoparticles (i.e., 20, 60, and 100 nm) were

466 generated by a atomizer. Different from generation conditions of for 6-10 nm ammonium sulfate
467 nanoparticles in Biskos et al. (2006b), in our study, in order to minimize the multiple charged nanoparticles,

468 three different concentrations are used so that the size selected by the nano-DMA1 (i.e., 6, 8, 10 nm) was

Deleted: es

Formatted: Font color: Text 1

Formatted: Font color: Text 1

Deleted:

Formatted: Font color: Text 1

471 always slight larger than peak of the number size distribution of the generated nanoparticles by the
472 electrospray. This also helps us to have as many as nanoparticles as possible to compensate the strong
473 nanoparticle losses in the nano-HTDMA system. In addition, we used both electrospray and atomizer to
474 generate 20-nm ammonium sulfate, and compared their hygroscopic growth factors prior to deliquescence.
475 Figure S12a shows a ~ 0.1 higher growth factor of 20-nm ammonium sulfate generated by the electrospray
476 than that using the atomizer in the RH range from 55% to 82%, which is similar to the difference in
477 hygroscopic growth factor of 20-nm NaCl aerosol nanoparticles using the different generation method as
478 observed in Fig S12b in Biskos et al. (2006a). Besides different generation conditions, the morphology of
479 dried ammonium sulfate particles may also differ slightly between our study and Biskos et al. (2006)
480 because of different drying rate, as drying flow rates and RH of the dried ammonium sulfate in the two
481 HTDMA systems are different too. This means the different generation methods and drying conditions may
482 influence the surface structure of the nanoparticles and thus their interaction with the adsorbed water layers
483 (Iskandar et al., 2003; Xin et al., 2019).

484 **3.2 Size-dependent hygroscopicity of sodium sulfate nanoparticles**

485 As a common constituent of atmospheric aerosol particles (Tang and Munkelwitz, 1993, 1994; Tang 1996;
486 Tang et al., 2007), hygroscopicity of sodium sulfate with diameters above 20 nm particles has been
487 investigated by a few groups (Tang et al., 2007; Xu and Schweiger, 1999; Hu et al., 2010). However, its
488 hygroscopic behavior in the sub-10 nm size range has not been investigated yet. In this study, we applied
489 our nano-HTDMA system to measure the hygroscopic growth factors, DRH, and ERH of sodium sulfate
490 nanoparticles with dry size from 20 nm down to 6 nm.

491 Figure 9 shows the measured size-resolved hygroscopic growth factors of sodium sulfate nanoparticles.
492 Different from the observations by Tang et al. (2007) using an electrodynamic balance (EDB), we observed
493 prompt deliquescence and efflorescence for both 20-nm and 6-nm sodium sulfate nanoparticles. Two
494 intersecting modes in the measured number size distribution of humidified sodium sulfate nanoparticles is

495 observed at RH close to the DRH (Fig. S9 and S10 in the Supplementary Information) and ERH, suggesting
496 an externally mixed of aqueous and solid nanoparticles. As shown in Sect. 3.1.3, a similar phenomenon is
497 also observed for ammonium sulfate, which could be attributed to the slight RH heterogeneities in nano-
498 DMA2, which makes only part of the nanoparticles deliquesce at RH close to the DRH, while the others
499 remain in solid state.

500 Together with the hygroscopic growth of 14-16 μm and 200-20 nm sodium sulfate measured previously by
501 Tang et al. (2007) and Hu et al. (2010), we show a strong size dependence in hygroscopic growth factors
502 of sodium sulfate nanoparticles (Fig. S11d). For example, at RH 84%, the hygroscopic growth factor of 6
503 nm sodium sulfate is only ~ 1.3 (in efflorescence mode), while the respective growth factors are about 1.5
504 and 1.8 for 20 nm and 14-16 μm particles. As shown in Fig. 9, E-AIM already agrees well with the
505 hygroscopic growth of micrometer particles (14-16 μm) without shape correction (DeCarlo et al., 2004),
506 i.e., shape factor (χ) of 1.0. However, to explain observation, a shape factor of ~ 1.16 and 1.26 would be
507 needed for 20 nm and 6 nm sodium sulfate nanoparticles, respectively.

508 There is no significant change in DRH between 14-16 μm ($\sim 84\%$) and 20 nm ($\sim 84\%$) sodium sulfate
509 particles (Fig. 9). This is consistent with Hu et al. (2010) where no change in DRH from 200 nm down to
510 20 nm ($\sim 82\%$, see Table 1 from Hu et al. (2010)) was observed. However, a significant increase of DRH
511 occurred when further decreasing particle diameters to 6 nm (DRH = $\sim 90\%$). The size dependence of ERH
512 is stronger than that of DRH, as there is already a clear increase of ERH from micrometer 14-16 μm ($\sim 57\%$)
513 to 20 nm ($\sim 62\%$) sodium sulfate particles. When further reducing the particle diameters to 6 nm, an almost
514 6% increase of DRH can be found, compared to the micrometer 14-16 μm particles (i.e., ERH increases

515 from 57 to 82%, respectively). Different from ammonium sulfate, of which DRH and ERH shows no
516 significant size dependence, there is a strong size-dependence of DRH and ERH of sodium sulfate
517 according to our observations down to 6 nm. The different size dependence of DRH and ERH between
518 sodium chloride and ammonium sulfate have been theoretically studied and explained by Cheng et al.

Deleted:

Formatted: Font color: Text 1

520 (2015). The main reason is the different concentration dependence of solute activities and the different
521 solute-liquid surface tension, e.g., the same change in solute molality leads to a larger change in the solute
522 activity of sodium chloride than that of ammonium sulfate. The phase transition concentration
523 (deliquescence and crystallization concentration) of ammonium sulfate is thus more sensitive to the size
524 change compared to that of sodium chloride, leading to the almost unchanged DRH and ERH of ammonium
525 sulfate nanoparticles (Cheng et al., 2015). For the size dependence of phase transition of sodium sulfate, a
526 strong size effect on DRH and ERH is similar to that of sodium chloride but different from that of
527 ammonium sulfate in the size range from 6 to 20 nm, suggesting that non-ideality of solution property is
528 close to that of sodium chloride but weaker than that of ammonium sulfate. As different hydrates of sodium
529 sulfate may exist during the deliquescence and efflorescence processes (Xu and Schweiger, 1999), to
530 explain the underline mechanism of the size dependent hygroscopicity of sodium sulfate particles can be
531 challenging.

533 **4 Summary and Conclusion**

534 In this study, we presented our newly designed and self-assembled nano-HTDMA for measuring
535 hygroscopicity of nanoparticles in the sub-10 nm diameter size range. We also introduced the
536 comprehensive methods for system calibration and reported the performance of the system, focusing on the
537 sizing accuracy and preventing pre-deliqescence in the deliquescence measurement mode. By comparing
538 with previous studies on ammonium sulfate nanoparticles (Biskos et al., 2006b), we show that our system
539 is capable of providing high quality data of the hygroscopic behavior of sub-10 nm nanoparticles. We then
540 extended our measurements for sodium sulfate nanoparticles, of which size-dependent deliquescence and
541 efflorescence have been clearly observed for nanoparticles down to 6 nm in size, with similar behavior as
542 sodium chloride.

Deleted: The strong size-effect on the DRH and ERH of sodium chloride and on hygroscopic growth factors of ammonium sulfate have been observed by Biskos et al. (2006a, b, 2007) and theoretically studied and explained by Cheng et al. (2015). Owing to the strong non-ideality of aqueous ammonium sulfate solution, the phase transition concentration (deliquescence and crystallization concentration) of ammonium sulfate is much more sensitivity to the size changes from 60 nm to 6 nm than that of sodium chloride, leading to the almost unchanged DRH and ERH of ammonium sulfate nanoparticles (Cheng et al., 2015). Compared the three compounds, the size-dependent hygroscopicity of sodium sulfate nanoparticles from 20 nm to 6 nm is similar to that of sodium chloride, but different to that of ammonium sulfate, where no significant change in DRH and ERH was observed. However, in this size range, the increase of the ERH and the decrease of growth factor upon decreasing size seems to be stronger for sodium sulfate than sodium chloride, although no significant change in DRH was observed from micrometer size particles down to 20 nm.

563 As we know, atmospheric aerosol particles consist of not only inorganic components, but also a vast number
564 of organic components existing in the atmosphere. However, their physico-chemical properties are still not
565 fully understood, especially when comes to the nano-scale and supersaturated concentration range. The
566 nano-HTDMA system can be directly applicable to explore the size dependence of aerosol nanoparticles.
567 Combing the multi-size measurements of hygroscopicity and the Differential Köhler Analyses (DKA,
568 Cheng et al., 2015) in nano size range, we will be able characterize and parameterize the water activity and
569 surface tension of different inorganic and organic systems. This will further help us to understand the
570 formation and transformation of aerosol nanoparticles in the atmosphere and their interaction with water
571 vapor.

572 **Data availability**

573 Readers who are interested in the data should contact Yafang Cheng (yafang.cheng@mpic.de).

574 **Acknowledgement**

575 This study was supported by the Max Planck Society (MPG) and Leibniz Society. T.L. acknowledges the
576 support from China Scholarship Council (CSC). Y.C. would like to acknowledge the Minerva Program of
577 MPG.

578 **Author contributions:** Y.C. and H.S. designed and led the study. N.M., T.T. and A. W. assembled the
579 basic HTDMA system. Y.C., H.S. and T.L. modified and advanced the basic system into the nano-HTDMA
580 for the purpose of measuring hygroscopic properties of aerosol nanoparticles in sub-10 nm size range at
581 MPIC. T.L. performed the experiments. J.H., N.M. and X.W. supported the experiments. All co-authors
582 discussed the results and commented on the manuscript. T.L. wrote the manuscript with input from all co-
583 authors.

584

585 **Reference**

586 Andreae, M. O., Afchine, A., Albrecht, R., Holanda, B. A., Artaxo, P., Barbosa, H. M. J., Borrmann, S.,
587 Cecchini, M. A., Costa, A., Dollner, M., Fütterer, D., Järvinen, E., Jurkat, T., Klimach, T., Konemann, T.,
588 Knote, C., Krämer, M., Krisna, T., Machado, L. A. T., Mertes, S., Minikin, A., Pöhlker, C., Pöhlker, M. L.,
589 Pöschl, U., Rosenfeld, D., Sauer, D., Schlager, H., Schnaiter, M., Schneider, J., Schulz, C., Spanu, A.,
590 Sperling, V. B., Voigt, C., Walser, A., Wang, J., Weinzierl, B., Wendisch, M., and Ziereis, H.: Aerosol
591 characteristics and particle production in the upper troposphere over the Amazon Basin, *Atmos. Chem.*
592 *Phys.*, 18, 921-961, 2018.

593 [Atkins, P., De Paula, J., and Walters, V.: Physical Chemistry, W. H. Freeman, 2006.](#)

594 Badger, C. L., George, I., Griffiths, P. T., Braban, C. F., Cox, R. A., and Abbatt, J. P. D.: Phase transitions
595 and hygroscopic growth of aerosol particles containing humic acid and mixtures of humic acid and
596 ammonium sulphate, *Atmospheric Chemistry and Physics*, 6, 755-768, 2006.

597 Bezantakos, S., Huang, L., Barmounis, K., Martin, S. T., and Biskos, G.: Relative humidity non-
598 uniformities in Hygroscopic Tandem Differential Mobility Analyzer measurements, *Journal of Aerosol*
599 *Science*, 101, 1-9, 2016.

600 Birmili, W., Stratmann, F., Wiedensohler, A., Covert, D., M. Russell, L., and Berg, O.: Determination of
601 Differential Mobility Analyzer Transfer Functions Using Identical Instruments in Series, 1997.

602 Birmili, W., Weinhold, K., Rasch, F., Sonntag, A., Sun, J., Merkel, M., Wiedensohler, A., Bastian, S.,
603 Schladitz, A., Löschau, G., Cyrys, J., Pitz, M., Gu, J., Kusch, T., Flentje, H., Quass, U., Kaminski, H.,
604 Kuhlbusch, T. A. J., Meinhardt, F., and Fiebig, M.: Long-term observations of tropospheric particle number
605 size distributions and equivalent black carbon mass concentrations in the German Ultrafine Aerosol
606 Network (GUAN), 2016.

Deleted: ¶

Formatted: Font color: Text 1

Formatted: Line spacing: 1,5 lines

614 Biskos, G., Malinowski, A., Russell, L. M., Buseck, P. R., and Martin, S. T.: Nanosize Effect on the
615 Deliquescence and the Efflorescence of Sodium Chloride Particles, *Aerosol Science and Technology*, 40,
616 97-106, 2006a.

617 Biskos, G., Paulsen, D., Russell, L. M., Buseck, P. R., and Martin, S. T.: Prompt deliquescence and
618 efflorescence of aerosol nanoparticles, *Atmospheric Chemistry and Physics*, 6, 4633-4642, 2006b.

619 Biskos, G., Russell, L. M., Buseck, P. R., and Martin, S. T.: Nanosize effect on the hygroscopic growth
620 factor of aerosol particles, *Geophysical Research Letters*, 33, 2007.

621 Chan, M. N. and Chan, C. K.: Hygroscopic properties of two model humic-like substances and their
622 mixtures with inorganics of atmospheric importance, *Environmental Science & Technology*, 37, 5109-
623 5115, 2003.

624 Chan, M. N. and Chan, C. K.: Mass transfer effects in hygroscopic measurements of aerosol particles,
625 *Atmospheric Chemistry and Physics*, 2005.

626 Chan, M. N., Kreidenweis, S. M., and Chan, C. K.: Measurements of the Hygroscopic and Deliquescence
627 Properties of Organic Compounds of Different Solubilities in Water and Their Relationship with Cloud
628 Condensation Nuclei Activities, *Environmental Science & Technology*, 42, 3602-3608, 2008.

629 Chen, Da-Ren, David Y.H. Pui, and Stanley L. Kaufman.: Electrospinning of conducting liquids for
630 monodisperse aerosol generation in the 4 nm to 1.8 μm diameter range, *J. Aerosol Sci.*, 26: 963-977, 1995.

631 Cheng, Y., Su, H., Koop, T., Mikhailov, E., and Pöschl, U.: Size dependence of phase transitions in aerosol
632 nanoparticles, *Nature communications*, 6, 5923, 2015.

633 [Cheng, Y., Zheng, G., Wei, C., Mu, Q., Zheng, B., Wang, Z., Gao, M., Zhang, Q., He, K., Carmichael, G.,](#)
634 [Pöschl, U., and Su, H.: Reactive nitrogen chemistry in aerosol water as a source of sulfate during haze](#)
635 [events in China, *Science Advances*, 2, e1601530, 2016.](#)

Formatted: Font color: Text 1

636 Cheng, Y. F., Berghof, M., Garland, R. M., Wiedensohler, A., Wehner, B., Muller, T., Su, H., Zhang, Y.
637 H., Achtert, P., Nowak, A., Poschl, U., Zhu, T., Hu, M., and Zeng, L. M.: Influence of soot mixing state on
638 aerosol light absorption and single scattering albedo during air mass aging at a polluted regional site in
639 northeastern China, *Journal of Geophysical Research-Atmospheres*, 114, 2009.

640 Cheng, Y. F., Wiedensohler, A., Eichler, H., Heintzenberg, J., Tesche, M., Ansmann, A., Wendisch, M.,
641 Su, H., Althausen, D., Herrmann, H., Gnauk, T., Brüggemann, E., Hu, M., and Zhang, Y. H.: Relative
642 humidity dependence of aerosol optical properties and direct radiative forcing in the surface boundary layer
643 at Xinken in Pearl River Delta of China: An observation based numerical study, *Atmospheric Environment*,
644 42, 6373-6397, 2008.

645 Clegg, S. L., Brimblecombe, P., and Wexler, A. S.: Thermodynamic Model of the System $\text{H}^+ - \text{NH}_4^+ - \text{SO}_4^{2-}$
646 $- \text{NO}_3^- - \text{H}_2\text{O}$ at Tropospheric Temperatures, *The Journal of Physical Chemistry A*, 102, 2137-2154, 1998.

647 Collins, D. R., Cocker, D. R., Flagan, R. C., and Seinfeld, J. H.: The Scanning DMA Transfer Function,
648 *Aerosol Science and Technology*, 38, 833-850, 2004.

649 Cruz, C. N. and Pandis, S. N.: Deliquescence and Hygroscopic Growth of Mixed Inorganic–Organic
650 Atmospheric Aerosol, *Environmental Science & Technology*, 34, 4313-4319, 2000.

651 DeCarlo, P. F., Slowik, J. G., Worsnop, D. R., Davidovits, P., and Jimenez, J. L.: Particle Morphology and
652 Density Characterization by Combined Mobility and Aerodynamic Diameter Measurements. Part 1:
653 Theory, *Aerosol Science and Technology*, 38, 1185-1205, 2004.

654 Dong, J. L., Xiao, H. S., Zhao, L. J., and Zhang, Y.-H.: Spatially resolved Raman investigation on phase
655 separations of mixed $\text{Na}_2\text{SO}_4/\text{MgSO}_4$ droplets, 2009.

656 Dougle, P. G., Veefkind, J. P., and ten Brink, H. M.: Crystallisation of mixtures of ammonium nitrate,
657 ammonium sulphate and soot, *Journal of Aerosol Science*, 29, 375-386, 1998.

Deleted: ¶

659 Dunne, E. M., Gordon, H., Kürten, A., Almeida, J., Duplissy, J., Williamson, C., Ortega, I. K., Pringle, K.
660 J., Adamov, A., Baltensperger, U., Barmet, P., Benduhn, F., Bianchi, F., Breitenlechner, M., Clarke, A.,
661 Curtius, J., Dommen, J., Donahue, N. M., Ehrhart, S., Flagan, R. C., Franchin, A., Guida, R., Hakala, J.,
662 Hansel, A., Heinritzi, M., Jokinen, T., Kangasluoma, J., Kirkby, J., Kulmala, M., Kupc, A., Lawler, M. J.,
663 Lehtipalo, K., Makhmutov, V., Mann, G., Mathot, S., Merikanto, J., Miettinen, P., Nenes, A., Onnela, A.,
664 Rap, A., Reddington, C. L. S., Riccobono, F., Richards, N. A. D., Rissanen, M. P., Rondo, L., Sarnela, N.,
665 Schobesberger, S., Sengupta, K., Simon, M., Sipilä, M., Smith, J. N., Stozkhov, Y., Tomé, A., Tröstl, J.,
666 Wagner, P. E., Wimmer, D., Winkler, P. M., Worsnop, D. R., and Carslaw, K. S.: Global atmospheric
667 particle formation from CERN CLOUD measurements, *Science*, 354, 1119-1124, 2016.

668 Duplissy, J., Gysel, M., S, S., Meyer, N., N, G., L, K., V, M., R, W., Martins dos Santos, S., C, G., Villani,
669 P., P, L., Sellegri, K., A, M., B. McFiggans, G., G, W., R, R., Dommen, J., Ristovski, Z., and Weingartner,
670 E.: Intercomparison study of six HTDMAs: results and general recommendations for HTDMA operation,
671 *Atmospheric Measurement Techniques*, 2. Pp, 363-378, 2009.

672 Ehn, M., Thornton, J. A., Kleist, E., Sipilä, M., Junninen, H., Pullinen, I., Springer, M., Rubach, F.,
673 Tillmann, R., Lee, B., Lopez-Hilfiker, F., Andres, S., Acir, I.-H., Rissanen, M., Jokinen, T., Schobesberger,
674 S., Kangasluoma, J., Kontkanen, J., Nieminen, T., Kurtén, T., Nielsen, L. B., Jørgensen, S., Kjaergaard, H.
675 G., Canagaratna, M., Maso, M. D., Berndt, T., Petäjä, T., Wahner, A., Kerminen, V.-M., Kulmala, M.,
676 Worsnop, D. R., Wildt, J., and Mentel, T. F.: A large source of low-volatility secondary organic aerosol,
677 *Nature*, 506, 476, 2014.

678 Eichler, H., Cheng, Y., Birmili, W., Nowak, A., Wiedensohler, A., Brüggemann, E., Gnauk, T., Herrmann,
679 H., Althausen, D., Ansmann, A., Engelmann, R., Tesche, M., Wendisch, M., Zhang, Y. H., Hu, M., Liu, S.,
680 and Zeng, L.: Hygroscopic properties and extinction of aerosol particles at ambient relative humidity in
681 South-Eastern China, 2008.

682 Estillore, A. D., Morris, H. S., Or, V. W., Lee, H. D., Alves, M. R., Marciano, M. A., Laskina, O., Qin, Z.,
683 Tivanski, A. V., and Grassian, V. H.: Linking hygroscopicity and the surface microstructure of model
684 inorganic salts, simple and complex carbohydrates, and authentic sea spray aerosol particles, *Physical*
685 *Chemistry Chemical Physics*, 19, 21101-21111, 2017.

686 Fan, J., Rosenfeld, D., Zhang, Y., Giangrande, S. E., Li, Z., Machado, L. A. T., Martin, S. T., Yang, Y.,
687 Wang, J., Artaxo, P., Barbosa, H. M. J., Braga, R. C., Comstock, J. M., Feng, Z., Gao, W., Gomes, H. B.,
688 Mei, F., Pöhlker, C., Pöhlker, M. L., Pöschl, U., and de Souza, R. A. F.: Substantial convection and
689 precipitation enhancements by ultrafine aerosol particles, *Science*, 359, 411-418, 2018.

690 Gao, Y., Chen, S. B., and Yu, L. E.: Efflorescence Relative Humidity for Ammonium Sulfate Particles,
691 *The Journal of Physical Chemistry A*, 110, 7602-7608, 2006.

692 Ghorai, S., Wang, B., Tivanski, A., and Laskin, A.: Hygroscopic Properties of Internally Mixed Particles
693 Composed of NaCl and Water-Soluble Organic Acids, *Environmental Science & Technology*, 48, 2234-
694 2241, 2014.

695 Giamarelou, M., Smith, M., Papapanagiotou, E., Martin, S. T., and Biskos, G.: Hygroscopic properties of
696 potassium-halide nanoparticles, *Aerosol Science and Technology*, 52, 536-545, 2018.

697 Gysel, M., Weingartner, E., and Baltensperger, U.: Hygroscopicity of aerosol particles at low temperatures.
698 2. Theoretical and experimental hygroscopic properties of laboratory generated aerosols, *Environmental*
699 *Science & Technology*, 36, 63-68, 2002.

700 Hämeri, K., Laaksonen, A., Väkevä, M., and Suni, T.: Hygroscopic growth of ultrafine sodium chloride
701 particles, *Journal of Geophysical Research: Atmospheres*, 106, 20749-20757, 2001.

702 Hämeri, K., Väkevä, M., Hansson, H.-C., and Laaksonen, A.: Hygroscopic growth of ultrafine ammonium
703 sulfate aerosol measured using an ultrafine tandem differential mobility analyzer, *Journal of Geophysical*
704 *Research: Atmospheres*, 105, 22231-22242, 2000.

705 Hansson, H.-C., Rood, M. J., Koloutsou-Vakakis, S., Hämeri, K., Orsini, D., and Wiedensohler, A.: NaCl
706 Aerosol Particle Hygroscopicity Dependence on Mixing with Organic Compounds, *Journal of Atmospheric*
707 *Chemistry*, 31, 321-346, 1998.

708 Hennig, T., Massling, A., Brechtel, F. J., and Wiedensohler, A.: A tandem DMA for highly temperature-
709 stabilized hygroscopic particle growth measurements between 90 % and 98% relative humidity, *Journal of*
710 *Aerosol Science*, 36, 1210-1223, 2005.

711 Hong, J., Häkkinen, S. A. K., Paramonov, M., Äijälä, M., Hakala, J., Nieminen, T., Mikkilä, J., Prisle, N.
712 L., Kulmala, M., Riipinen, I., Bilde, M., Kerminen, V. M., and Petäjä, T.: Hygroscopicity, CCN and
713 volatility properties of submicron atmospheric aerosol in a boreal forest environment during the summer
714 of 2010, *Atmos. Chem. Phys.*, 14, 4733-4748, 2014.

715 Hong, J., Kim, J., Nieminen, T., Duplissy, J., Ehn, M., Äijälä, M., Hao, L. Q., Nie, W., Sarnela, N., Prisle,
716 N. L., Kulmala, M., Virtanen, A., Petäjä, T., and Kerminen, V. M.: Relating the hygroscopic properties of
717 submicron aerosol to both gas- and particle-phase chemical composition in a boreal forest environment,
718 *Atmos. Chem. Phys.*, 15, 11999-12009, 2015.

719 Hu, D., Qiao, L., Chen, J.-M., Ye, X., Yang, X., Cheng, T., and Fang, W.: Hygroscopicity of Inorganic
720 Aerosols: Size and Relative Humidity Effects on the Growth Factor, 2010.

721 Iskandar, F., Gradon, L., and Okuyama, K.: Control of the morphology of nanostructured particles prepared
722 by the spray drying of a nanoparticle sol, *Journal of Colloid and Interface Science*, 265, 296-303, 2003.

723 Kerminen, V. M.: The effects of particle chemical character and atmospheric processes on particle
724 hygroscopic properties, *Journal of Aerosol Science*, 28, 121-132, 1997.

725 Keskinen, H., Virtanen, A., Joutsensaari, J., Tsagkogeorgas, G., Duplissy, J., Schobesberger, S., Gysel, M.,
726 Riccobono, F., Slowik, J. G., Bianchi, F., Yli-Juuti, T., Lehtipalo, K., Rondo, L., Breitenlechner, M., Kupc,
727 A., Almeida, J., Amorim, A., Dunne, E. M., Downard, A. J., Ehrhart, S., Franchin, A., Kajos, M. K., Kirkby,
728 J., Kürten, A., Nieminen, T., Makhmutov, V., Mathot, S., Miettinen, P., Onnela, A., Petäjä, T., Praplan, A.,
729 Santos, F. D., Schallhart, S., Sipilä, M., Stozhkov, Y., Tomé, A., Vaattovaara, P., Wimmer, D., Prevot, A.,
730 Dommen, J., Donahue, N. M., Flagan, R. C., Weingartner, E., Viisanen, Y., Riipinen, I., Hansel, A.,
731 Curtius, J., Kulmala, M., Worsnop, D. R., Baltensperger, U., Wex, H., Stratmann, F., and Laaksonen, A.:
732 Evolution of particle composition in CLOUD nucleation experiments, *Atmos. Chem. Phys.*, 13, 5587-5600,
733 2013.

734 Kim, J., Ahlm, L., Yli-Juuti, T., Lawler, M., Keskinen, H., Tröstl, J., Schobesberger, S., Duplissy, J.,
735 Amorim, A., Bianchi, F., Donahue, N. M., Flagan, R. C., Hakala, J., Heinritzi, M., Jokinen, T., Kürten, A.,
736 Laaksonen, A., Lehtipalo, K., Miettinen, P., Petäjä, T., Rissanen, M. P., Rondo, L., Sengupta, K., Simon,
737 M., Tomé, A., Williamson, C., Wimmer, D., Winkler, P. M., Ehrhart, S., Ye, P., Kirkby, J., Curtius, J.,
738 Baltensperger, U., Kulmala, M., Lehtinen, K. E. J., Smith, J. N., Riipinen, I., and Virtanen, A.:
739 Hygroscopicity of nanoparticles produced from homogeneous nucleation in the CLOUD experiments,
740 *Atmos. Chem. Phys.*, 16, 293-304, 2016.

741 [Kinney, P. D., Pui, D. Y. H., Mullholland, G. W. & Bryner, N. P. Use of the Electrostatic Classification](#)
742 [Method to Size 0.1 µm SRM Particles—A Feasibility Study. *Journal of Research of the National Institute*](#)
743 [of Standards and Technology.](#), 96, 147, 1991.

744 ~~Kirkby, J., Curtius, J., Almeida, J., Dunne, E., Duplissy, J., Ehrhart, S., Franchin, A., Gagné, S., Ickes, L.,~~
745 Kürten, A., Kupc, A., Metzger, A., Riccobono, F., Rondo, L., Schobesberger, S., Tsagkogeorgas, G.,
746 Wimmer, D., Amorim, A., Bianchi, F., Breitenlechner, M., David, A., Dommen, J., Downard, A., Ehn, M.,

Formatted: Font color: Text 1

Deleted: ¶

748 Flagan, R. C., Haider, S., Hansel, A., Hauser, D., Jud, W., Junninen, H., Kreissl, F., Kvashin, A.,
749 Laaksonen, A., Lehtipalo, K., Lima, J., Lovejoy, E. R., Makhmutov, V., Mathot, S., Mikkilä, J., Minginette,
750 P., Mogo, S., Nieminen, T., Onnela, A., Pereira, P., Petäjä, T., Schnitzhofer, R., Seinfeld, J. H., Sipilä, M.,
751 Stozhkov, Y., Stratmann, F., Tomé, A., Vanhanen, J., Viisanen, Y., Vrtala, A., Wagner, P. E., Walther, H.,
752 Weingartner, E., Wex, H., Winkler, P. M., Carslaw, K. S., Worsnop, D. R., Baltensperger, U., and Kulmala,
753 M.: Role of sulphuric acid, ammonia and galactic cosmic rays in atmospheric aerosol nucleation, *Nature*,
754 476, 429-433, 2011.

755 [Knutson, E. O. and Whitby, K. T.: Aerosol classification by electric mobility: apparatus, theory, and](#)
756 [applications. *Journal of Aerosol Science.*, 6, 443-451, 1975.](#)

757 Köhler, H.: The nucleus in and the growth of hygroscopic droplets, *Transactions of the Faraday Society*,
758 32, 1152-1161, 1936.

759 Kreidenweis, S. M., Koehler, K., DeMott, P. J., Prenni, A. J., Carrico, C., and Ervens, B.: Water activity
760 and activation diameters from hygroscopicity data - Part I: Theory and application to inorganic salts,
761 *Atmospheric Chemistry and Physics*, 5, 1357-1370, 2005.

762 Lei, T., Zuend, A., Cheng, Y., Su, H., Wang, W., and Ge, M.: Hygroscopicity of organic surrogate
763 compounds from biomass burning and their effect on the efflorescence of ammonium sulfate in mixed
764 aerosol particles, *Atmos. Chem. Phys.*, 18, 1045-1064, 2018.

765 Lei, T., Zuend, A., Wang, W. G., Zhang, Y. H., and Ge, M. F.: Hygroscopicity of organic compounds from
766 biomass burning and their influence on the water uptake of mixed organic ammonium sulfate aerosols,
767 *Atmos. Chem. Phys.*, 14, 11165-11183, 2014.

768 Lihavainen, H., Kerminen, V.-M., Komppula, M., Hatakka, J., Aaltonen, V., Kulmala, M., and Viisanen,
769 Y.: Production of “potential” cloud condensation nuclei associated with atmospheric new-particle
770 formation in northern Finland, *Journal of Geophysical Research: Atmospheres*, 108, 2003.

Formatted: Font color: Text 1

771 Martin, S. T.: Phase Transitions of Aqueous Atmospheric Particles, *Chemical Reviews*, 100, 3403-3454,
772 2000.

773 Massling, A., Niedermeier, N., Hennig, T., Fors, E. O., Swietlicki, E., Ehn, M., Hämeri, K., Villani, P., Laj,
774 P., Good, N., McFiggans, G., and Wiedensohler, A.: Results and recommendations from an
775 intercomparison of six Hygroscopicity-TDMA systems, *Atmos. Meas. Tech.*, 4, 485-497, 2011.

776 McMurry, P. H.: A review of atmospheric aerosol measurements, *Atmospheric Environment*, 34, 1959-
777 1999, 2000.

778 Mikhailov, E., Vlasenko, S., Martin, S. T., Koop, T., and Poschl, U.: Amorphous and crystalline aerosol
779 particles interacting with water vapor: conceptual framework and experimental evidence for restructuring,
780 phase transitions and kinetic limitations, *Atmospheric Chemistry and Physics*, 9, 9491-9522, 2009.

781 Mikhailov, E., Vlasenko, S., Niessner, R., and Poschl, U.: Interaction of aerosol particles composed of
782 protein and salts with water vapor: hygroscopic growth and microstructural rearrangement, *Atmospheric
783 Chemistry and Physics*, 4, 323-350, 2004.

784 Mikhailov, E., Vlasenko, S., Rose, D., and Pöschl, U.: Mass-based hygroscopicity parameter interaction
785 model and measurement of atmospheric aerosol water uptake, *Atmos. Chem. Phys.*, 13, 717-740, 2013.

786 Mikhailov, E. F. and Vlasenko, S. S.: High humidity tandem differential mobility analyzer for accurate
787 determination of aerosol hygroscopic growth, microstructure and activity coefficients over a wide range of
788 relative humidity, *Atmos. Meas. Tech. Discuss.*, <https://doi.org/10.5194/amt-2019-478>, in review, 2019.

789 Mikhailov, E. F., Vlasenko, S. S., and Ryshkevich, T. I.: Influence of chemical composition and
790 microstructure on the hygroscopic growth of pyrogenic aerosol, *Izvestiya, Atmospheric and Oceanic
791 Physics*, 44, 416-431, 2008.

792 Mirabel, P., Reiss, H., and Bowles, R. K.: A theory for the deliquescence of small particles, *The Journal of*
793 *Chemical Physics*, 113, 8200-8205, 2000.

794 Mochida, M. and Kawamura, K.: Hygroscopic properties of levoglucosan and related organic compounds
795 characteristic to biomass burning aerosol particles, *Journal of Geophysical Research-Atmospheres*, 109,
796 2004.

797 Mulholland, G. W., Donnelly, M. K., Hagwood, C. R., Kukuck, S. R., Hackley, V. A., and Pui, D. Y. H.:
798 Measurement of 100 nm and 60 nm Particle Standards by Differential Mobility Analysis, *Journal of*
799 *Research of the National Institute of Standards and Technology*, 111, 257-312, 2006.

800 Park, K., Kim, J.-S., and Miller, A. L.: A study on effects of size and structure on hygroscopicity of
801 nanoparticles using a tandem differential mobility analyzer and TEM, *Journal of Nanoparticle Research*,
802 11, 175-183, 2009.

803 Peng, C., Chow, A. H. L., and Chan, C. K.: Hygroscopic Study of Glucose, Citric Acid, and Sorbitol Using
804 an Electrodynamic Balance: Comparison with UNIFAC Predictions, *Aerosol Science and Technology*, 35,
805 753-758, 2001.

806 Pope, F. D., Dennis-Smith, B. J., Griffiths, P. T., Clegg, S. L., and Cox, R. A.: Studies of Single Aerosol
807 Particles Containing Malonic Acid, Glutaric Acid, and Their Mixtures with Sodium Chloride. I.
808 Hygroscopic Growth, *The Journal of Physical Chemistry A*, 114, 5335-5341, 2010.

809 Pruppacher, H. R. & Klett, J. D: *Microphysics of clouds and precipitation*, Kluwer Academic Publishers,
810 1997.

811 Rader, D. J. and McMurry, P. H.: Application of the tandem differential mobility analyzer to studies of
812 droplet growth or evaporation, *Journal of Aerosol Science*, 17, 771-787, 1986.

813 Raoux, S., Rettner, C. T., Jordan-Sweet, J. L., Kellock, A. J., Topuria, T., Rice, P. M., and Miller, D. C.:
814 Direct observation of amorphous to crystalline phase transitions in nanoparticle arrays of phase change
815 materials, *Journal of Applied Physics*, 102, 094305, 2007.

816 Reid, J. P., Dennis-Smith, B. J., Kwamena, N.-O. A., Miles, R. E. H., Hanford, K. L., and Homer, C. J.:
817 The morphology of aerosol particles consisting of hydrophobic and hydrophilic phases: hydrocarbons,
818 alcohols and fatty acids as the hydrophobic component, *Physical Chemistry Chemical Physics*, 13, 15559-
819 15572, 2011.

820 Richardson, C. B. and Spann, J.: Measurement of Water Cycle in a Levitated Ammonium Sulfate Particles,
821 1984.

822 Rickards, A. M. J., Miles, R. E. H., Davies, J. F., Marshall, F. H., and Reid, J. P.: Measurements of the
823 Sensitivity of Aerosol Hygroscopicity and the κ Parameter to the O/C Ratio, *The Journal of Physical*
824 *Chemistry A*, 117, 14120-14131, 2013.

825 Romakkaniemi, S., Hämeri, K., Väkevä, M., and Laaksonen, A.: Adsorption of Water on 8–15 nm NaCl
826 and (NH₄)₂SO₄ Aerosols Measured Using an Ultrafine Tandem Differential Mobility Analyzer, *The*
827 *Journal of Physical Chemistry A*, 105, 8183-8188, 2001.

828 Russell, L. M. and Ming, Y.: Deliquescence of small particles, *Journal of Chemical Physics*, 116, 311-321,
829 2002.

830 Sakurai, H., A. Fink, M., H. McMurry, P., Mauldin, R., F. Moore, K., N. Smith, J., and Eisele, F.:
831 Hygroscopicity and volatility of 4–10 nm particles during summertime atmospheric nucleation events in
832 urban Atlanta, 2005.

833 Seinfeld, J. H., and S. N. Pandis: *Atmospheric Chemistry and Physics: From Air Pollution to Climate*
834 *Change*, 2nd ed., John Wiley, New York, 2006.

835 Sihto, S. L., Mikkilä, J., Vanhanen, J., Ehn, M., Liao, L., Lehtipalo, K., Aalto, P. P., Duplissy, J., Petäjä,
836 T., Kerminen, V. M., Boy, M., and Kulmala, M.: Seasonal variation of CCN concentrations and aerosol
837 activation properties in boreal forest, *Atmos. Chem. Phys.*, 11, 13269-13285, 2011.

838 Stock, M., Cheng, Y. F., Birmili, W., Massling, A., Wehner, B., Müller, T., Leinert, S., Kalivitis, N.,
839 Mihalopoulos, N., and Wiedensohler, A.: Hygroscopic properties of atmospheric aerosol particles over the
840 Eastern Mediterranean: implications for regional direct radiative forcing under clean and polluted
841 conditions, *Atmos. Chem. Phys.*, 11, 4251-4271, 2011.

842 Su, H., Rose, D., Cheng, Y. F., Gunthe, S. S., Massling, A., Stock, M., Wiedensohler, A., Andreae, M. O.,
843 and Pöschl, U.: Hygroscopicity distribution concept for measurement data analysis and modeling of aerosol
844 particle mixing state with regard to hygroscopic growth and CCN activation, *Atmos. Chem. Phys.*, 10,
845 7489-7503, 2010.

846 Tang, I. N.: Chemical and size effects of hygroscopic aerosols on light scattering coefficients, *Journal of*
847 *Geophysical Research: Atmospheres*, 101, 19245-19250, 1996.

848 Tang, I. N., Fung, K. H., Imre, D. G., and Munkelwitz, H. R.: Phase Transformation and Metastability of
849 Hygroscopic Microparticles, *Aerosol Science and Technology*, 23, 443-453, 2007.

850 Tang, I. N. and Munkelwitz, H. R.: Composition and temperature dependence of the deliquescence
851 properties of hygroscopic aerosols, *Atmospheric Environment. Part A. General Topics*, 27, 467-473, 1993.

852 Tang, I. N. and Munkelwitz, H. R.: Water activities, densities, and refractive indices of aqueous sulfates
853 and sodium nitrate droplets of atmospheric importance, *Journal of Geophysical Research: Atmospheres*,
854 99, 18801-18808, 1994.

855 Tang, M., Chan, C. K., Li, Y. J., Su, H., Ma, Q., Wu, Z., Zhang, G., Wang, Z., Ge, M., Hu, M., He, H., and
856 Wang, X.: A review of experimental techniques for aerosol hygroscopicity studies, *Atmos. Chem. Phys.*,
857 19, 12631-12686, 2019.

858 Topping, D., McFiggans, G., and Coe, H.: A curved multi-component aerosol hygroscopicity model
859 framework: Part 1–Inorganic compounds, Atmospheric Chemistry and Physics, 5, 1205-1222, 2005.

860 Taylor, J. R. and Taylor, S. L. L. J. R.: Introduction To Error Analysis: The Study of Uncertainties in
861 Physical Measurements, University Science Books, 1997.

Formatted: Font color: Text 1

862 Villani, P., Picard, D., Michaud, V., Laj, P., and Wiedensohler, A.: Design and Validation of a Volatility
863 Hygroscopic Tandem Differential Mobility Analyzer (VH-TDMA) to Characterize the Relationships
864 Between the Thermal and Hygroscopic Properties of Atmospheric Aerosol Particles, Aerosol Science and
865 Technology, 42, 729-741, 2008.

Formatted: Normal, Justified

Deleted: ¶

Formatted: Font: (Default) Times New Roman, 12 pt

866 Vlasenko, S. S., Su, H., Pöschl, U., Andreae, M. O., and Mikhailov, E. F.: Tandem configuration of
867 differential mobility and centrifugal particle mass analysers for investigating aerosol hygroscopic
868 properties, Atmos. Meas. Tech., 10, 1269-1280, 2017.

869 Wang, J., Krejci, R., Giangrande, S., Kuang, C., Barbosa, H. M. J., Brito, J., Carbone, S., Chi, X.,
870 Comstock, J., Ditas, F., Lavric, J., Manninen, H. E., Mei, F., Moran-Zuloaga, D., Pöhlker, C., Pöhlker, M.
871 L., Saturno, J., Schmid, B., Souza, R. A. F., Springston, S. R., Tomlinson, J. M., Toto, T., Walter, D.,
872 Wimmer, D., Smith, J. N., Kulmala, M., Machado, L. A. T., Artaxo, P., Andreae, M. O., Petäjä, T., and
873 Martin, S. T.: Amazon boundary layer aerosol concentration sustained by vertical transport during rainfall,
874 Nature, 539, 416, 2016.

875 Wang, L., Khalizov, A. F., Zheng, J., Xu, W., Ma, Y., Lal, V., and Zhang, R.: Atmospheric nanoparticles
876 formed from heterogeneous reactions of organics, Nature Geoscience, 3, 238, 2010.

877 Wang, X., Ma, N., Lei, T., Groß, J., Li, G., Liu, F., Meusel, H., Mikhailov, E., Wiedensohler, A., and Su,
878 H.: Effective density and hygroscopicity of protein particles generated with spray-drying process, Journal
879 of Aerosol Science, 137, 105441, 2019.

881 Wang, Z., Su, H., Wang, X., Ma, N., Wiedensohler, A., Pöschl, U., and Cheng, Y.: Scanning
882 supersaturation condensation particle counter applied as a nano-CCN counter for size-resolved analysis of
883 the hygroscopicity and chemical composition of nanoparticles, *Atmos. Meas. Tech.*, 8, 2161-2172,
884 <https://doi.org/10.5194/amt-8-2161-2015>, 2015.

885 Wiedensohler, A., Birmili, W., Nowak, A., Sonntag, A., Weinhold, K., Merkel, M., Wehner, B., Tuch, T.,
886 Pfeifer, S., Fiebig, M., Fjåraa, A. M., Asmi, E., Sellegri, K., Depuy, R., Venzac, H., Villani, P., Laj, P.,
887 Aalto, P., Ogren, J. A., Swietlicki, E., Williams, P., Roldin, P., Quincey, P., Hüglin, C., Fierz-
888 Schmidhauser, R., Gysel, M., Weingartner, E., Riccobono, F., Santos, S., Gröning, C., Faloon, K.,
889 Beddows, D., Harrison, R., Monahan, C., Jennings, S. G., O'Dowd, C. D., Marinoni, A., Horn, H. G., Keck,
890 L., Jiang, J., Scheckman, J., McMurry, P. H., Deng, Z., Zhao, C. S., Moerman, M., Henzing, B., de Leeuw,
891 G., Löschau, G., and Bastian, S.: Mobility particle size spectrometers: harmonization of technical standards
892 and data structure to facilitate high quality long-term observations of atmospheric particle number size
893 distributions, *Atmos. Meas. Tech.*, 5, 657-685, 2012.

894 Wiedensohler, A., Cheng, Y. F., Nowak, A., Wehner, B., Achtert, P., Berghof, M., Birmili, W., Wu, Z. J.,
895 Hu, M., Zhu, T., Takegawa, N., Kita, K., Kondo, Y., Lou, S. R., Hofzumahaus, A., Holland, F., Wahner,
896 A., Gunthe, S. S., Rose, D., Su, H., and Pöschl, U.: Rapid aerosol particle growth and increase of cloud
897 condensation nucleus activity by secondary aerosol formation and condensation: A case study for regional
898 air pollution in northeastern China, *Journal of Geophysical Research: Atmospheres*, 114, 2009.

899 Wiedensohler, A., Wiesner, A., Weinhold, K., Birmili, W., Hermann, M., Merkel, M., Müller, T., Pfeifer,
900 S., Schmidt, A., Tuch, T., Velarde, F., Quincey, P., Seeger, S., and Nowak, A.: Mobility particle size
901 spectrometers: Calibration procedures and measurement uncertainties, *Aerosol Science and Technology*,
902 52, 146-164, 2018.

903 Wise, M. E., Surratt, J. D., Curtis, D. B., Shilling, J. E., and Tolbert, M. A.: Hygroscopic growth of
904 ammonium sulfate/dicarboxylic acids, *Journal of Geophysical Research-Atmospheres*, 108, 2003.

905 Wu, Z. J., Nowak, A., Poulain, L., Herrmann, H., and Wiedensohler, A.: Hygroscopic behavior of
906 atmospherically relevant water-soluble carboxylic salts and their influence on the water uptake of
907 ammonium sulfate, *Atmos. Chem. Phys.*, 11, 12617-12626, 2011.

908 Xu, B. and Schweiger, G.: In-situ Raman observation of phase transformation of Na₂SO₄ during the
909 hydration/dehydration cycles on single levitated microparticle, 1999.

910 You, Y., Renbaum-Wolff, L., and Bertram, A. K.: Liquid-liquid phase separation in particles containing
911 organics mixed with ammonium sulfate, ammonium bisulfate, ammonium nitrate or sodium chloride,
912 *Atmos. Chem. Phys.*, 13, 11723-11734, 2013.

913 Zawadowicz, M. A., Proud, S. R., Seppalainen, S. S., and Cziczo, D. J.: Hygroscopic and phase separation
914 properties of ammonium sulfate/organics/water ternary solutions, *Atmos. Chem. Phys.*, 15, 8975-8986,
915 2015.

916 Zhang, S. L., Ma, N., Kecorius, S., Wang, P. C., Hu, M., Wang, Z. B., Größ, J., Wu, Z. J., and Wiedensohler,
917 A.: Mixing state of atmospheric particles over the North China Plain, *Atmospheric Environment*, 125, 152-
918 164, 2016.

919 Zhao, L.-J., Zhang, Y.-H., Wei, Z.-F., Cheng, H., and Li, X.-H.: Magnesium Sulfate Aerosols Studied by
920 FTIR Spectroscopy: Hygroscopic Properties, Supersaturated Structures, and Implications for Seawater
921 Aerosols, *The Journal of Physical Chemistry A*, 110, 951-958, 2006.

922 Zheng, G. J., Duan, F. K., Su, H., Ma, Y. L., Cheng, Y., Zheng, B., Zhang, Q., Huang, T., Kimoto, T.,
923 Chang, D., Pöschl, U., Cheng, Y. F., and He, K. B.: Exploring the severe winter haze in Beijing: the impact
924 of synoptic weather, regional transport and heterogeneous reactions, *Atmos. Chem. Phys.*, 15, 2969-2983,
925 2015.

926

Formatted: Font color: Text 1

Deleted: ¶

¶
¶
¶
¶
¶
¶
¶
¶
¶
¶

941 **Tables**942 **Table 1.** Accuracy, precision and sources of uncertainty associated with HTDMA measurements.

	Biskos et al. (2006b)	Hämeri et al. (2000)	Nano-HTDMA (This study)
<i>DMA System</i>			
Type of DMA1 & DMA2	TSI nano-DMAs	Hauke-type DMAs	Vienna-type short DMAs
Accuracy of aerosol flow in DMA2	±1% (0.3-1.5 l/min)	-	±1% (1.5 l/min)
Accuracy of sheath flow in DMA2	±1% (5-15 l/min)	-	±1% (10 l/min)
Accuracy of DMA voltage	±0.1% (0-500V)	-	±0.1% (0-350V)
Sizing accuracy of DMA2 using PSL	3%	-	0.4% (100-nm PSL)
Sizing agreement between DMAs using ammonium sulfate	3.1% (10 nm) ^a	±1% ^b	0.6% (100 nm) ^c 0.5% (60 nm) ^c 1.4% (20 nm) ^c 0.9% (10 nm) ^c -0.2% (8 nm) ^c 1.4% (6 nm) ^c
Precision of particle-sizing	<2%	-	<2% (6-200 nm) ^d

Humidification System			
Type of RH sensor	RH sensors (Omega Model HX93AV)	Dew point mirror (GE) RH sensors (Vaisala Humitter model 50Y)	Dew point mirror (Edge) RH sensors (Vaisala model HMT 330)
Accuracy of RH sensors (0-90% RH)	±2.5% RH	±3% RH ^e	±1% (RH sensor)
Position of the probe in the system	Inlet of DMA2 (RH _a sensor ^f , RH _s sensor ^g)	Inlet of DMA2 (RH _a sensor) & excess air (RH _s sensor, dew point mirror)	Inlet of DMA2 (RH _a sensor, RH _s sensor) & excess air (dew point mirror)
RH setting	RH _a =RH _s	RH _s ≥ RH _a +3%	RH _a =RH _s
Temperature Control System			
Temperature control type	Thermally isolated environment (humidification+DMA2) ^h	Thermally isolated environment (DMA2)	Box T regulated (humidification+DMA2)
Difference in T between inlet and outlet of DMA2	-	-	<0.2°C

943 ^aNot reported.

944 ^aAccording to the scans of the second DMA for the hygroscopic growth of 10 nm ammonium sulfate and the growth factors at different RHs provided by Biskos et al. (2006b), we retrieved an average sizing offset of Biskos et al. (2006b) system to be ~3.1% at 10 nm (see SI, S1).

945 ^bSize range not given.

946 ^cSee Table S2 in supporting information.

947 ^dValue calculated according to the relative standard derivation.

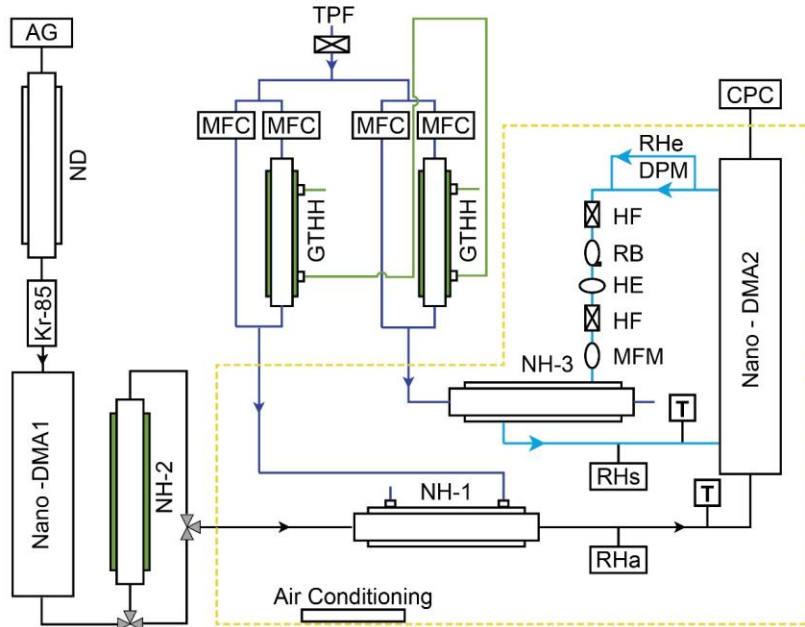
948 ^eFrom Vaisala Humitter model 50Y manual.

949 ^fRH_a: the RH of aerosol flow.

950 ^gRH_s: the RH of sheath flow.

951 ^hBezantakos et al. (2016).

952



954

955 **Figure 1.** Experimental setup of the nano-HTDMA. Here, AG: aerosol generator (aerosol atomizer or electrospray);
 956 ND: nafion dryer; Kr-85: Krypton source aerosol neutralizer; Nano-DMA: nano differential mobility analyzer; TPF:
 957 total particle filter; HF: hydrophobic filter; MFC: mass flow controller; MFM: mass flow meter; RB: recirculation
 958 blower; DPM: dew point mirror; GTHH: Gore-Tex humidifier and heater; NH: nafion humidifier; HE: heat exchanger;
 959 CPC: condensation particle counter; Black line: aerosol line; Blue line: sheath line; Royal blue line: humidified air;
 960 Green line: MilliQ water (resistivity of 18.2 MΩ cm at 298.15 K). RH_a and RH_s (measured by RH sensors) represent
 961 the RH of aerosol and sheath flow in the inlet of nano-DMA2, respectively. RH_e (measured by dew point) represents
 962 the RH of excess air. T represent the temperature of aerosol and sheath flow in the inlet of nano-DMA2, respectively.

963

964

965

Formatted: Centered

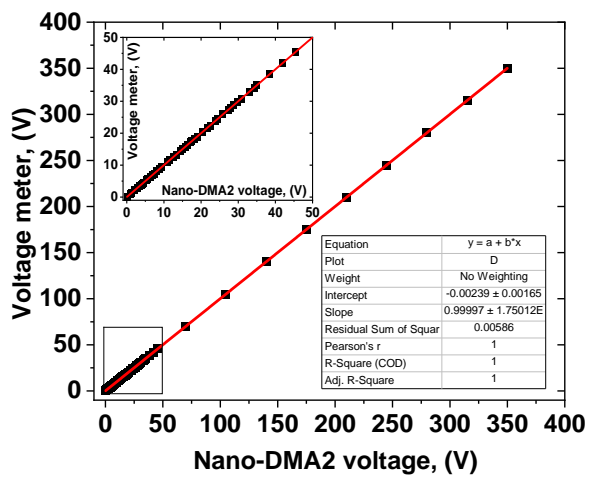


Figure 2. An example of voltage calibration of the nano-DMA2.

966

967

968

969

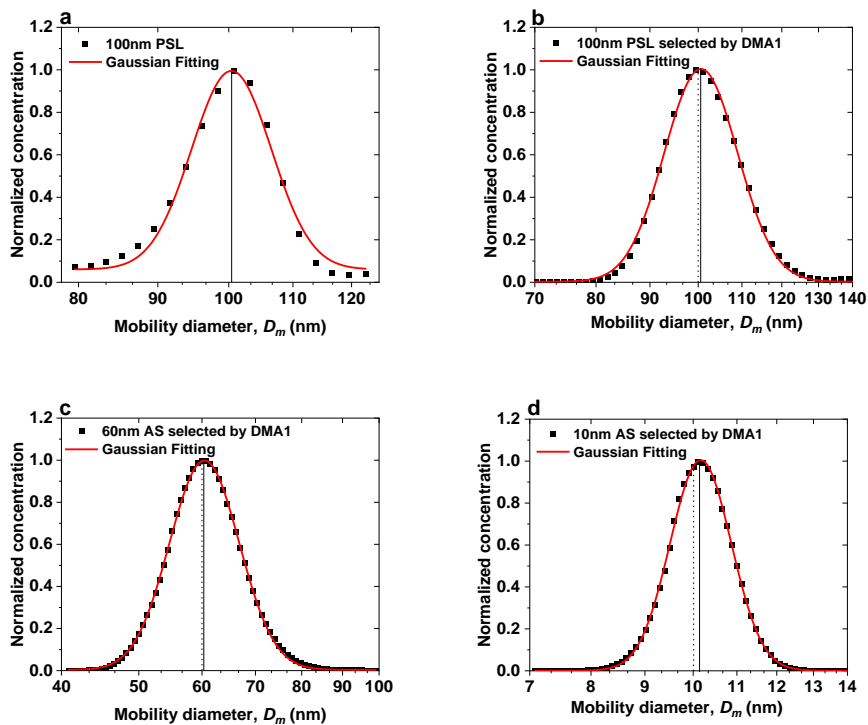
970

971

972

973

974

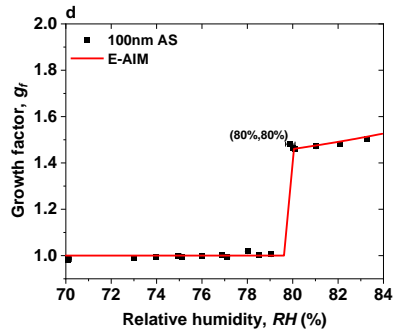
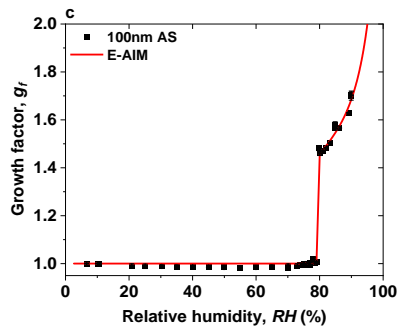
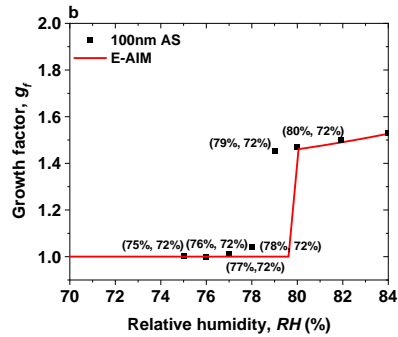
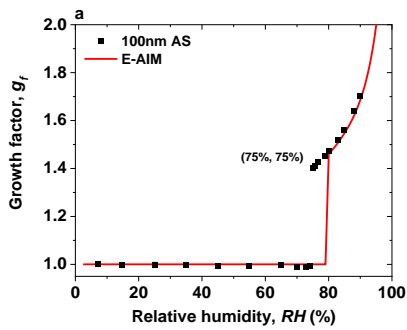


975

976

977 **Figure 3.** Sizing accuracy and sizing offset of nano-DMAs after calibration. (a) Normalized number size distribution
 978 scanned by the nano-DMA2 for 100-nm PSL nanoparticles (black solid square). The black solid line marks peak
 979 diameter from the Gaussian fits for the scan (red curve). Normalized number size distributions scanned by the nano-
 980 DMA2 for 100-nm PSL nanoparticles (b), 60-nm (c), and 10-nm (d) ammonium sulfate (AS) selected by the nano-
 981 DMA1 at RH below 5% at 298 K (black solid square). The dotted lines mark the diameters of the monodispersed
 982 nanoparticles selected by the nano-DMA1, i.e., 100 nm in (b), 60 nm in (c) and 10 nm in (d). The black solid lines
 983 mark the peak diameters from the Gaussian fits (red curve).

984



985

986

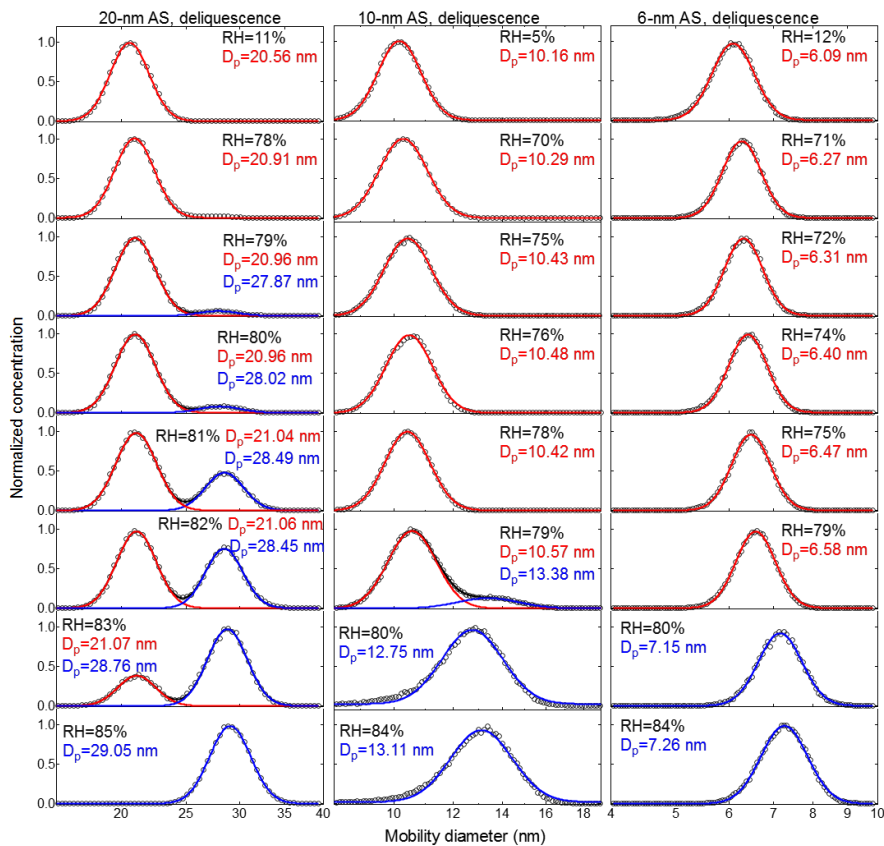
987 **Figure 4.** Mobility-diameter hygroscopic growth factors (g_f) of 100-nm ammonium sulfate (AS) nanoparticles at 298
 988 K measured in deliquescence mode. In comparison, the E-AIM model predicted growth factors of ammonium sulfate
 989 nanoparticles at 100 nm. (a) $RH_c = RH_a$, (75%, 75%) represents the (RH_c , RH_a), (b) $RH_c \geq RH_a + 3\%$, (75%, 72%)
 990 represents the (RH_c , RH_a), and (c) $RH_s = RH_a$. (d) The enlarged view of the RH range of 70% to 84% in Fig. 4c. (80%,
 991 80%) represents the (RH_s , RH_a). RH_s and RH_c are the RH of sheath flow in the inlet of nano-DMA2 and in the excess
 992 air line, respectively; RH_a is the RH of aerosol flow in the inlet of nano-DMA2.

993

994

995

996



Formatted: Centered

997

998 **Figure 5.** Deliquescence-mode measurements of ammonium sulfate (AS) aerosol nanoparticles with dry mobility

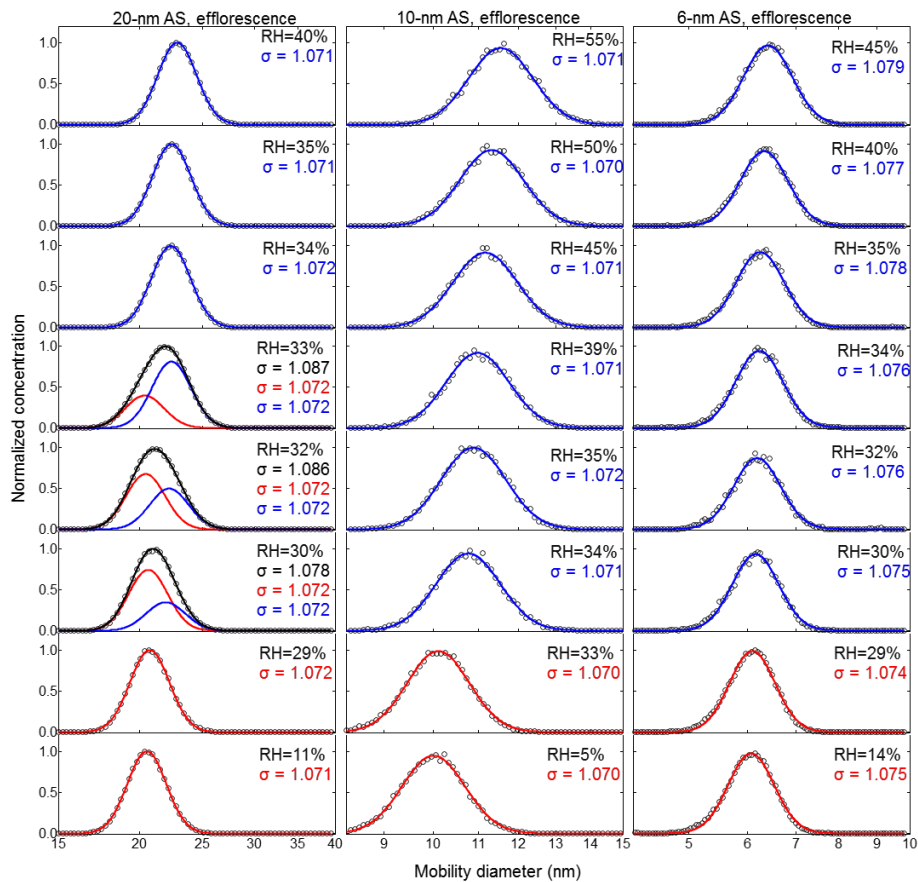
999 diameter from 20-6nm. The measured (black square) and fitted (solid lines) normalized size distribution are shown for

1000 increasing RH. The red and blue lines represent the aerosol nanoparticles in the solid and liquid state, respectively.

1001 The RH history in each measurement is 5% → X%, where X is the RH value given in each panel.

Formatted: Font color: Text 1

1002

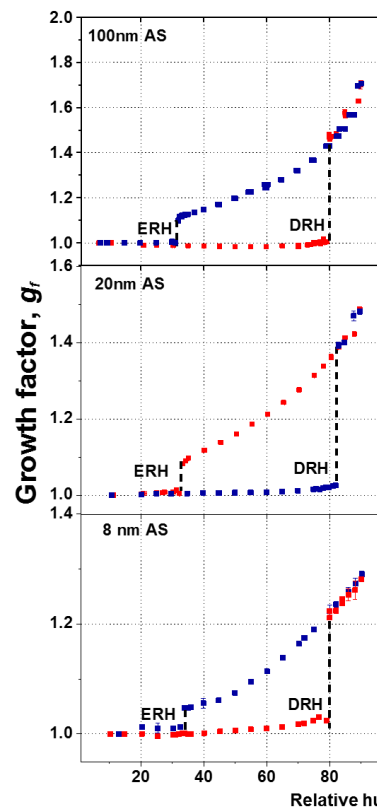
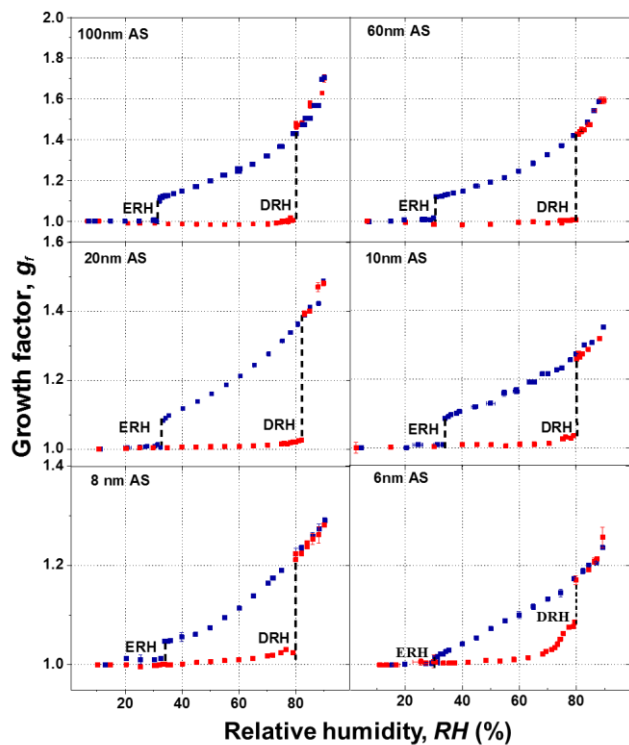


1003
 1004 **Figure 6.** Efflorescence-mode measurements of ammonium sulfate (AS) aerosol nanoparticles with dry mobility
 1005 diameter from 20-6nm. The measured (black circle) and fitted (solid lines) normalized size distribution are shown for
 1006 increasing RH. The red and blue lines represent the aerosol nanoparticles in the solid and liquid state, respectively.
 1007 The RH history in each measurement is 5%→97%→X%, where X is the RH value given in each panel.

Formatted: Centered

Formatted: Font color: Text 1

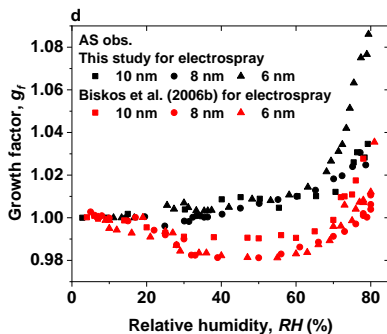
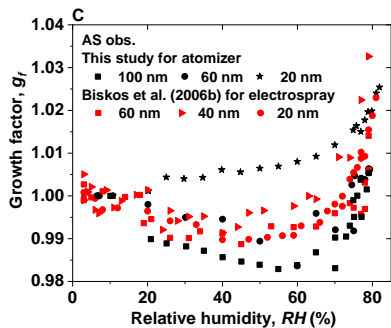
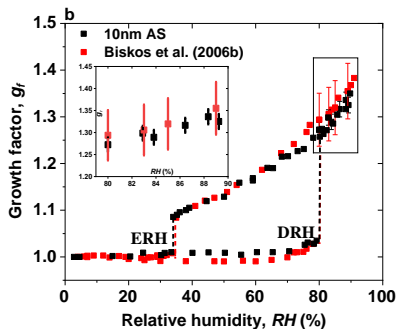
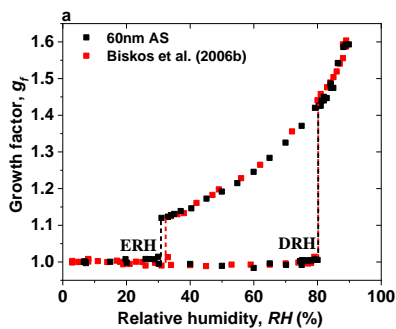
1008
 1009
 1010



Deleted:

1011
 1012 **Figure 7.** Mobility-diameter hygroscopic growth factors (g_r) of ammonium sulfate (AS) aerosol nanoparticles with dry
 1013 mobility diameter from 6 to 100 nm in the deliquescence mode (red square and error bar) and the efflorescence mode
 1014 (royal square and error bar). Deliquescence, and efflorescence relative humidity (DRH&ERH, black dashed line) of
 1015 ammonium sulfate (AS) nanoparticles with dry mobility diameter from 6 to 100 nm.

1016



1018

1019

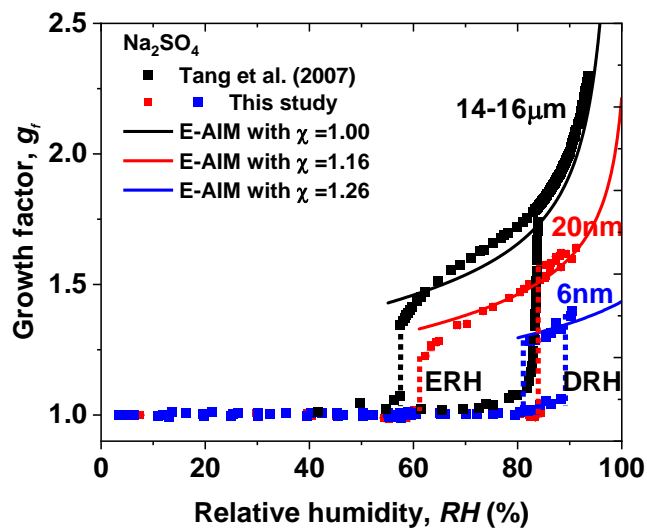
1020 **Figure 8. (a-b)** Mobility-diameter hygroscopic growth factors (g_f , black squares), deliquescence and efflorescence
 1021 relative humidity (DRH&ERH, black dashed lines) of ammonium sulfate (AS) nanoparticles with dry diameter 60 and
 1022 10 nm, respectively. Red squares and dashed lines show the respective results from Biskos et al. (2006b), respectively.

1023 Black and red uncertainties of growth factors at certain RH are calculated by $\sqrt{\left(\left(g_f \frac{\sqrt{2}\epsilon_{Dp}}{D_p}\right)^2 + \left(\epsilon_{RH} \frac{dg_f}{dRH}\right)^2\right)}$, where

1024 ϵ_{Dp} , ϵ_{RH} , and g_f are uncertainty of particle mobility diameter, uncertainty of relative humidity, and growth factor with
 1025 respect to RH, respectively (Mochida and Kawamura 2004). (c-d) Comparison of growth factors of ammonium sulfate
 1026 (AS) nanoparticles with dry diameter range from 6 to 100 nm with Biskos et al. (2006b) prior to deliquescence of
 1027 ammonium sulfate nanoparticles.

1028

1029



1030
 1031 **Figure 9.** Mobility-diameter hygroscopic growth factors (g_f), deliquescence and efflorescence relative humidity
 1032 (DRH&ERH, red and blue dashed lines) of sodium sulfate nanoparticles with dry diameter 20 (red square) and 6 (blue
 1033 square) nm, respectively. Black squares and dashed lines show the respective results from Tang et al. (2007) with
 1034 electrodynamic balance (EDB), respectively. In this study, the black, red, and blue curves show E-AIM predictions,
 1035 including the Kelvin effect and shape factors (χ).

1036
 1037
 1038
 1039
 1040
 1041
 1042

1 **Table S1:** Deliquescence and efflorescence relative humidity of ammonium sulfate below 100 nm reported by different studies in
 2 temperature ranging from 290-300K

Deliquescence relative humidity (DRH)	Efflorescence relative humidity (ERH)	Technique (initial particle size)	Reference
80-86%* (8 nm)		HTDMA	Hämeri et al. (2000)
80-85%* (10 nm)		(8,10,15,30,50 nm)	(cf. Figure 2a, 2b, 2c, 2d, and 2e)
80-90%* (15 nm)			
78-80%* (30 nm)			
76-79%* (50 nm)			
76-80%*	65%*	HTDMA (100 nm)	Gysel et al. (2002) (cf. Figure 2)
82% (6 nm)	34% (6 nm)	HTDMA	Biskos et al. (2006b)
81% (8 nm)	33% (8 nm)	(6,8,10,20,40,60 nm)	
80% (10 nm)	35% (10 nm)		
82% (20 nm)	35% (20 nm)		
80% (40 nm)	36% (40 nm)		
80% (60 nm)	33% (6 nm)		
-	27-31%* (43.7 nm)	HTDMA	Gao et al. (2006)
	21-30.7%* (47 nm)	(43.7,47 nm)	(cf. Figure 5)
78-81%*	-	HTDMA (100 nm)	Duplissy et al. (2009) (cf. Figure 4)
77-78%*	-	HTDMA	Duplissy et al. (2009)

Deleted:

		(100 nm)	(cf. Figure 4)
78-80%*	29-34%*	HTDMA (100 nm)	Mikhailov et al. (2009) (cf. Fig4)
77-78%	-	HTDMA (100 nm)	Wu et al. (2011)

4 -: Not reported

5 *: Data retrieved from figures in the references

6 80-86%: Non-prompt deliquescence of 8-nm ammonium sulfate from 80% to 86% RH

7 27-31%: Non-prompt efflorescence of 43.7-nm ammonium sulfate from 31% to 27% RH

8 82%: Prompt deliquescence of 6-nm ammonium sulfate at 82% RH

9

10

11

12

13 **Table S2.** Residence time (s) for the water equilibrium for particles with diameter ranging from 6
 14 to 100 nm particles at RH=90% at 25°C

χ	1	0.1	0.01	0.001
100nm	6.26×10^{-6}	3.55×10^{-5}	3.12×10^{-4}	0.0031
60nm	6.04×10^{-6}	3.34×10^{-5}	3.07×10^{-4}	0.0030
20nm	6.03×10^{-7}	5.17×10^{-6}	5.08×10^{-5}	5.07×10^{-4}
10nm	1.88×10^{-7}	1.74×10^{-6}	1.73×10^{-5}	1.72×10^{-4}
8nm	3.10×10^{-8}	1.93×10^{-7}	1.82×10^{-6}	1.81×10^{-5}
6nm	1.48×10^{-8}	1.08×10^{-7}	1.04×10^{-6}	1.03×10^{-5}

15
 16
 17

18 **Table S3.** Average sizing offset between nano-DMA2 in the nano-HTDMA system at RH below
 19 10%

	<u>Average sizing offset (nm)</u> ^a	Size agreement between nano-DMA1 and nano-DMA2 ^b
100-nm (NH ₄) ₂ SO ₄	0.619318	0.619318%
60-nm (NH ₄) ₂ SO ₄	0.298691	0.4978%
20-nm (NH ₄) ₂ SO ₄	0.278311	1.3916%
10-nm (NH ₄) ₂ SO ₄	0.089647	0.8965%
8-nm (NH ₄) ₂ SO ₄	-0.01598	-0.19975%
6-nm (NH ₄) ₂ SO ₄	0.083965	1.3994 %

- Formatted: Font color: Text 1
- Deleted: Offset(average)
- Formatted: Left
- Formatted Table
- Formatted: Left
- Formatted: Left
- Formatted: Left
- Formatted: Left
- Formatted: Left
- Formatted: Left

20 ^a Calculation from $(\bar{D}_{\text{measured by nano-DMA2}} - D_{\text{selected by nano-DMA1}})$

21 ^b Calculation from $[(\bar{D}_{\text{measured by nano-DMA2}} - D_{\text{selected by nano-DMA1}}) / D_{\text{selected by nano-DMA1}}] \times 100\%$

22
 23

25 **Table S4.** The values of D_m , g_i , and $D_m (< 5\% \text{ RH})$ of 10-nm ammonium sulfate of Biskos et al.
 26 (2006b) system in the different RHs.

Relative humidity	D_m	g_i	$D_m (< 5\% \text{ RH})$
<u>25%</u>	<u>10.3982439</u>	<u>0.992914120</u>	<u>10.47245043</u>
<u>76%</u>	<u>10.38867117</u>	<u>1.017488426</u>	<u>10.21011237</u>
<u>78%</u>	<u>10.54314064</u>	<u>1.027692308</u>	<u>10.25904404</u>
<u>80%</u>	<u>13.31036607</u>	<u>1.293796610</u>	<u>10.28783502</u>
<u>44%</u>	<u>11.56059002</u>	<u>1.120463542</u>	<u>10.31768513</u>
<u>35%</u>	<u>11.24527292</u>	<u>1.084064417</u>	<u>10.37325157</u>
<u>34%</u>	<u>10.59107394</u>	<u>1.007786565</u>	<u>10.50924304</u>
<u>32%</u>	<u>10.24542551</u>	<u>1.003831854</u>	<u>10.20631639</u>
<u>31%</u>	<u>10.20845456</u>	<u>1.001920937</u>	<u>10.18888236</u>
<u>30%</u>	<u>10.38101934</u>	<u>1.001441750</u>	<u>10.36607405</u>
<u>29%</u>	<u>10.27755951</u>	<u>1.003183756</u>	<u>10.2779752</u>
<u>24%</u>	<u>10.26077112</u>	<u>0.997295121</u>	<u>10.28860053</u>

Formatted: Font color: Text 1

Formatted: Font color: Text 1

27

28

Formatted: Font color: Text 1

29 **Table S5.** Uncertainties of nano-DMA voltage (V) and sheath flow rates (Q_{sh}), and calculated size
 30 uncertainty.

Size (nm)	Uncertainties in V and Q_{sh}	Uncertainty (Sizing accuracy)
<u>100</u>	<u>2648.2±0.02592* V, 10±0.02* L/min</u>	<u>0.2000%</u>
<u>60</u>	<u>1063.0±0.02686 V, 10±0.02 L/min</u>	<u>0.2000%</u>
<u>20</u>	<u>131.1±0.01519 V, 10±0.02L/min</u>	<u>0.2003%</u>
<u>10</u>	<u>33.7±0.02435 V, 10±0.02 L/min</u>	<u>0.2127%</u>
<u>8</u>	<u>21.6±0.03725 V, 10±0.02 L/min</u>	<u>0.2641%</u>
<u>6</u>	<u>12.2±0.06920 V, 10±0.02 L/min</u>	<u>0.6014%</u>

Formatted: Left

Formatted: Left

Formatted: Left

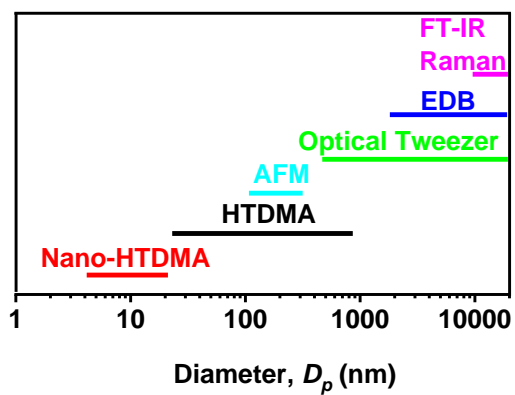
Formatted: Left

Formatted: Left

Formatted: Left

Formatted: Left

31



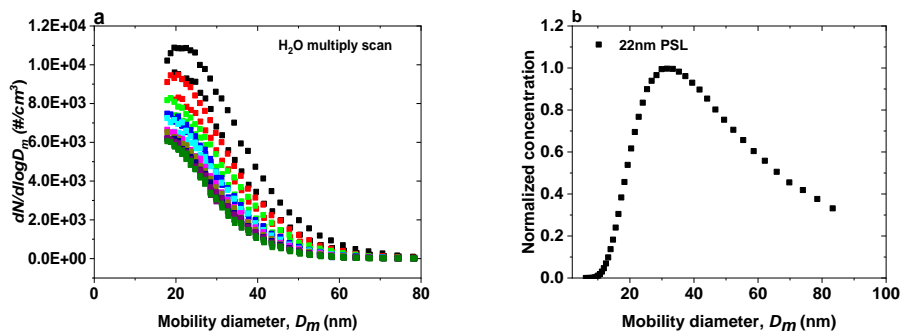
32
 33 **Figure S1.** Methods for measuring hygroscopicity of atmospheric aerosol particles in different size (D_p).

34

35

Deleted: ¶

36

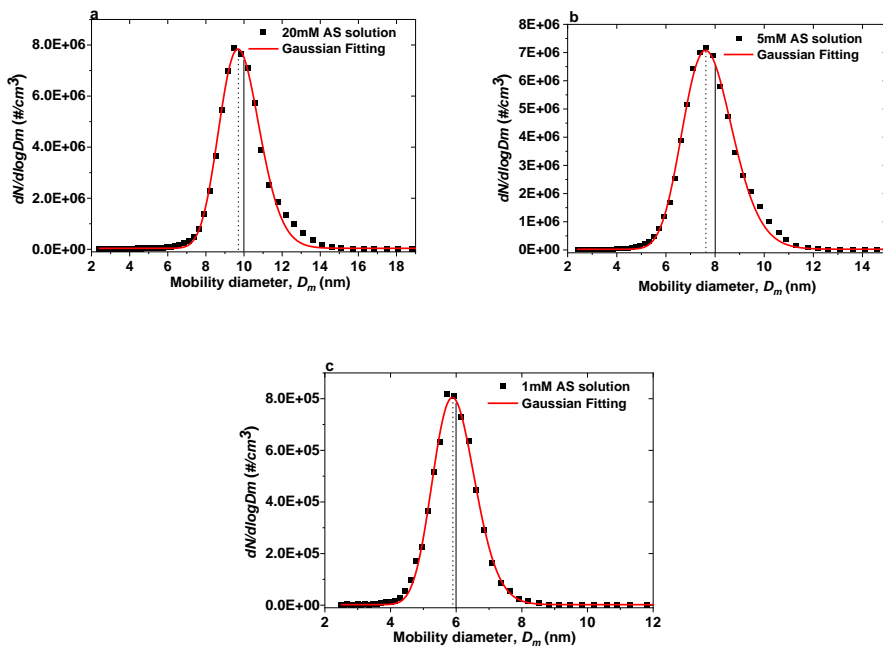


37

38

39 **Figure S2.** (a) Number concentration scanned for water nanoparticles by the nano-DMA2 at RH below 5% at 298 K.

40 (b) Normalized number size distribution scanned for 22-nm PSL nanoparticles by nano-DMA2 after calibration.



42

43

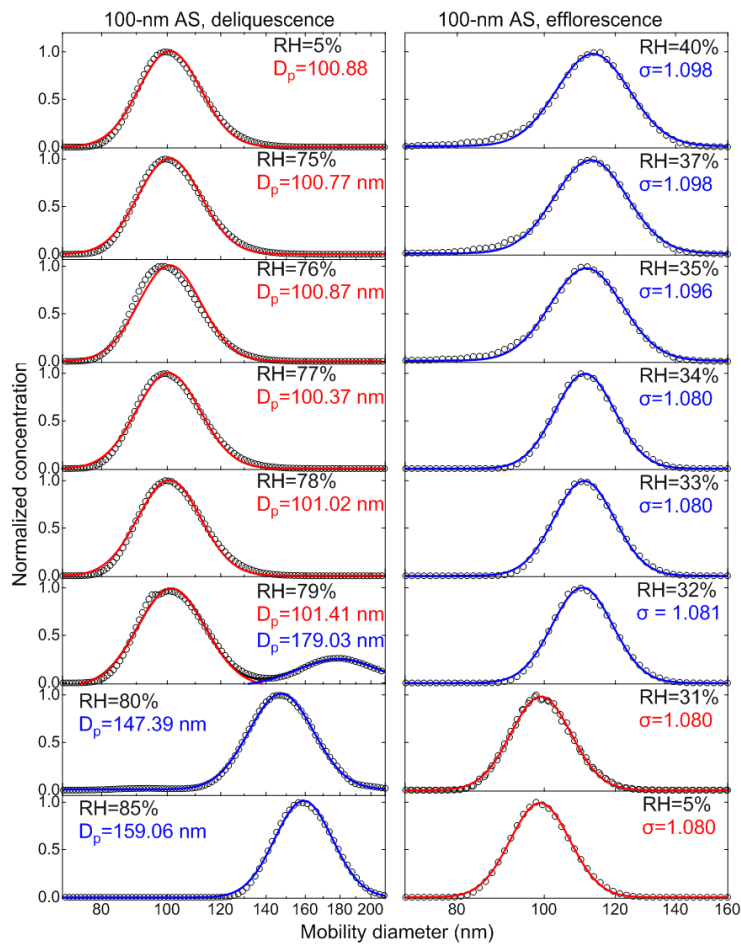
44

45 **Figure S3.** Number size distribution of ammonium sulfate (AS) nanoparticles (black solid square) generated by the
 46 electro spray. (a) 20mM, (b) 5mM, and (c) 1mM AS solution. The dotted line marks peak diameter from the Gaussian
 47 fits for the scan (red curve). The black solid lines mark the diameters of the monodispersed nanoparticles selected by
 48 the nano-DMA1.

49

50

51



52

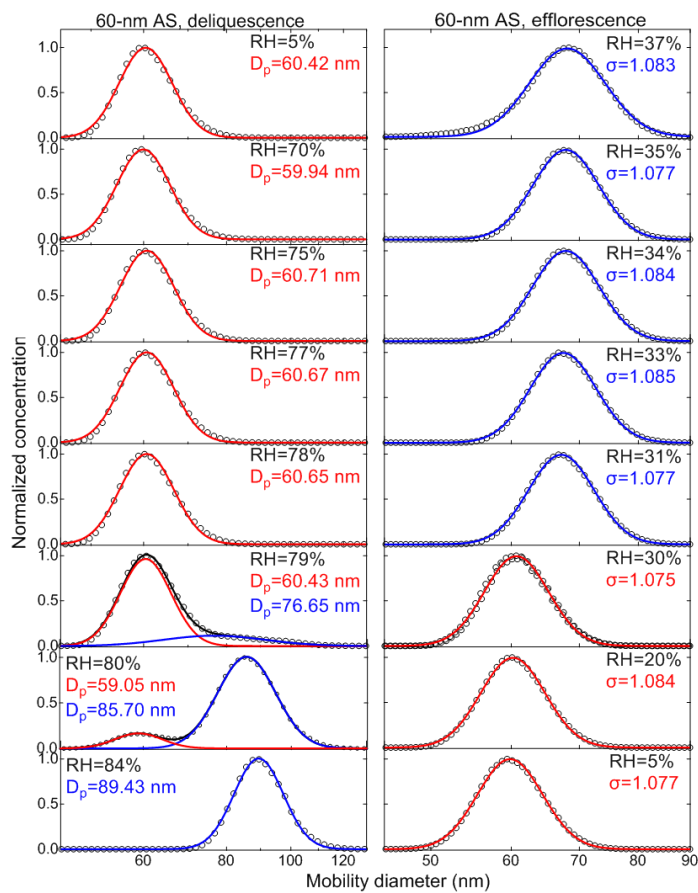
53

54 **Figure S4.** Deliquescence-mode (a) and efflorescence-mode (b) of 100-nm ammonium sulfate (AS) aerosol
 55 nanoparticles. The measured (black square) and fitted (solid lines) normalized size distribution are shown for
 56 increasing RH (5%→X%, where X is the RH value given in each panel) and decreasing RH (5%→97%→X%, where

57 X is the RH value given in each panel), respectively. The red and blue lines represent the aerosol nanoparticles in the
 58 solid and liquid state, respectively.

59

Formatted: Font color: Text 1

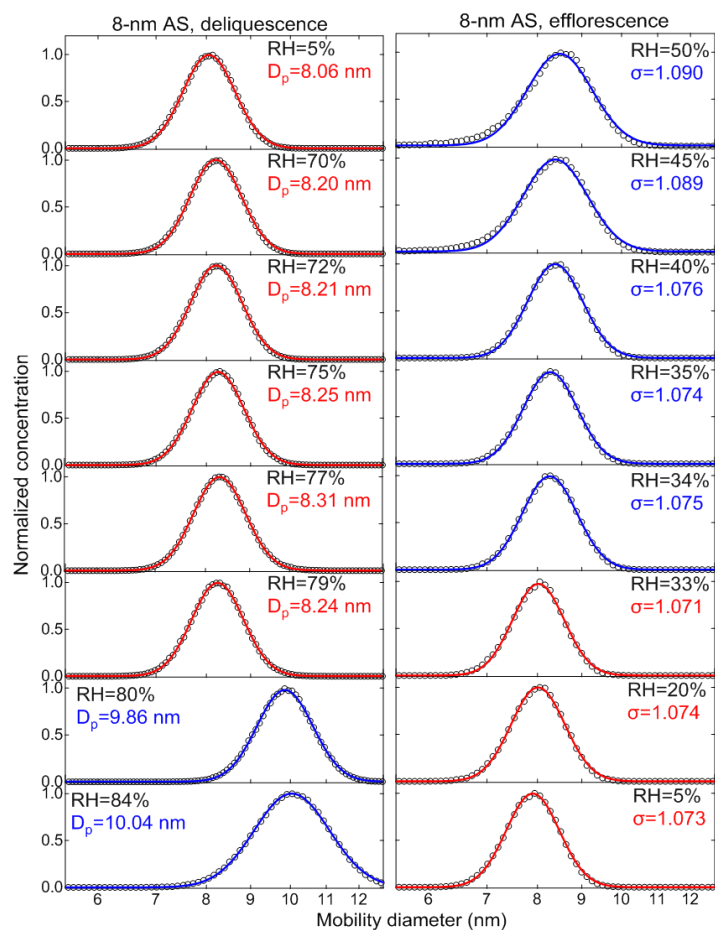


61

62

63 **Figure S5.** Deliquescence-mode (a) and efflorescence-mode (b) of 60-nm ammonium sulfate (AS) aerosol
 64 nanoparticles. The measured (black square) and fitted (solid lines) normalized size distribution are shown for
 65 increasing RH (5%→X%, where X is the RH value given in each panel) and decreasing RH (5%→97%→X%, where
 66 X is the RH value given in each panel), respectively. The red and blue lines represent the aerosol nanoparticles in the
 67 solid and liquid state, respectively.

Formatted: Font color: Text 1



69

70

71 **Figure S6.** Deliquescence-mode (a) and efflorescence-mode (b) of 8-nm ammonium sulfate (AS) aerosol nanoparticles.

72 The measured (black square) and fitted (solid lines, single-mode log-normal fit) normalized size distribution are shown

73 for increasing RH (5%→X%, where X is the RH value given in each panel) and decreasing RH (5%→97%→X%,

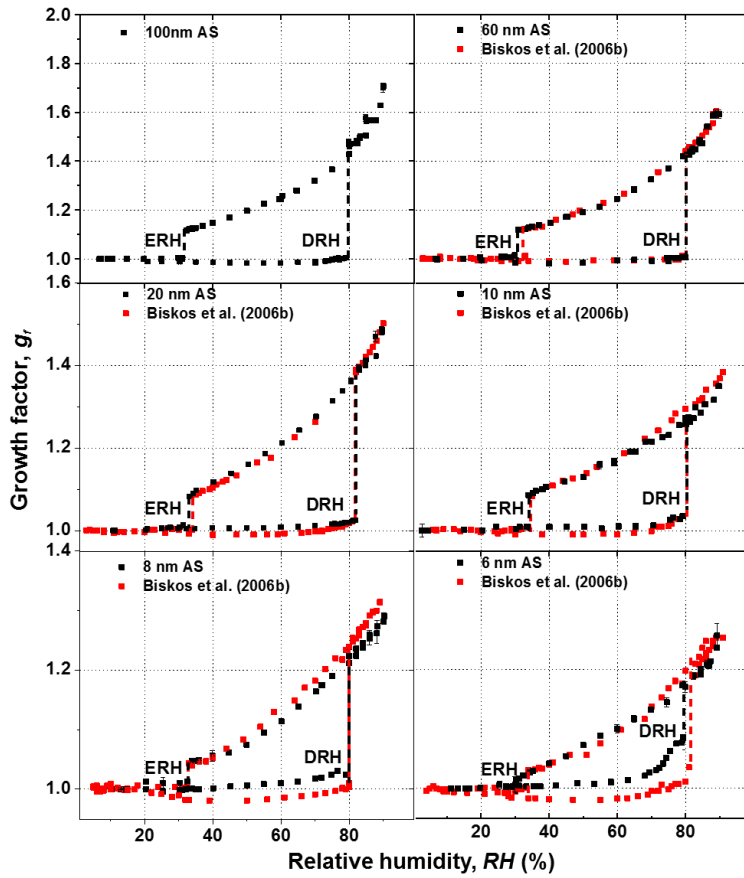
74 where X is the RH value given in each panel), respectively. The red and blue lines represent the aerosol nanoparticles

75 in the solid and liquid state, respectively.

Formatted: Font color: Text 1

76

77



78

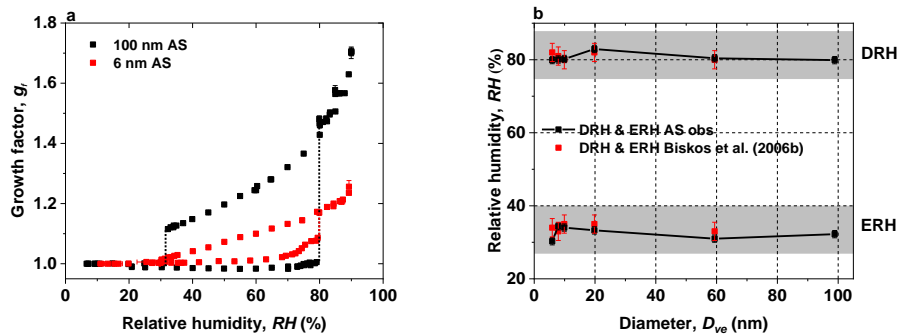
79

80 **Figure S7.** Mobility-diameter hygroscopic growth factors (g_r , black squares), deliquescence and efflorescence relative
81 humidity (DRH&ERH, black dashed lines) of ammonium sulfate (AS) nanoparticles with dry diameter from 6 to 100
82 nm, respectively. Red squares and dashed lines show the respective results from Biskos et al. (2006b),

Deleted: , respectively

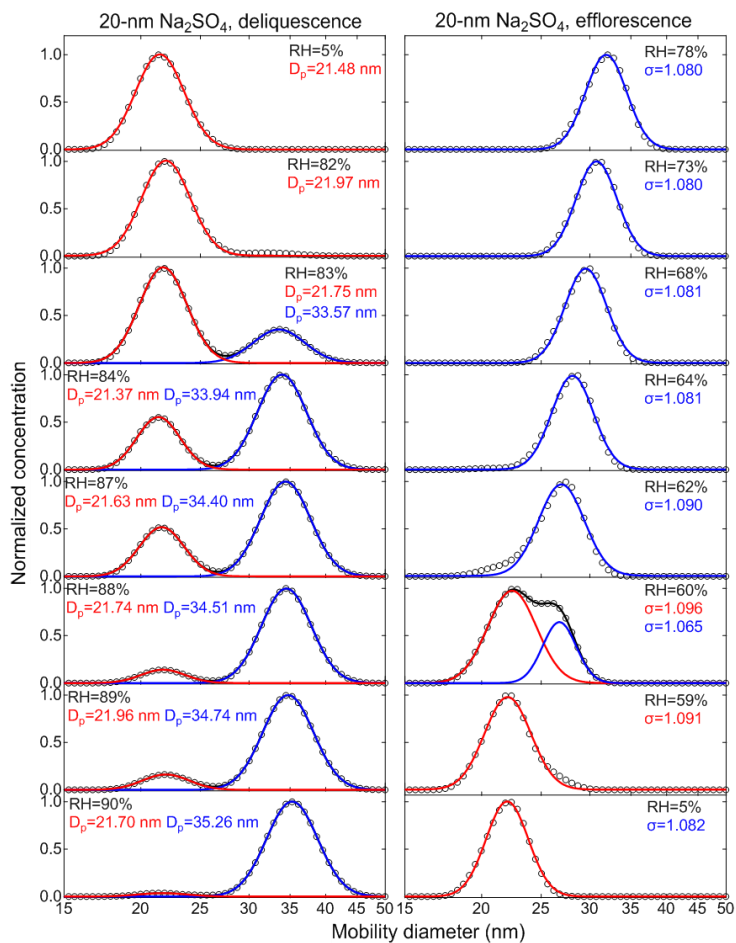
83

84



86
 87
 88 **Figure S8.** (a) Comparison of mobility-diameter hygroscopic growth factors (g_f) of 100-nm (black square) with 6-nm
 89 (red square) ammonium sulfate (AS) nanoparticles. (b) Dependence of deliquescence and efflorescence relative
 90 humidity (DRH&ERH) of ammonium sulfate (AS) on dry volume equivalent diameter (D_{ve}). The measured DRH and
 91 ERH of ammonium sulfate within RH uncertainty (black line + black square) compared with data from Biskos et al.
 92 (2006b) (red square) in the volume equivalent diameter with shape factor ($\chi=1.02$) range from 5 to 100 nm.

93
 94
 95
 96
 97
 98
 99
 100
 101
 102
 103
 104
 105
 106



107

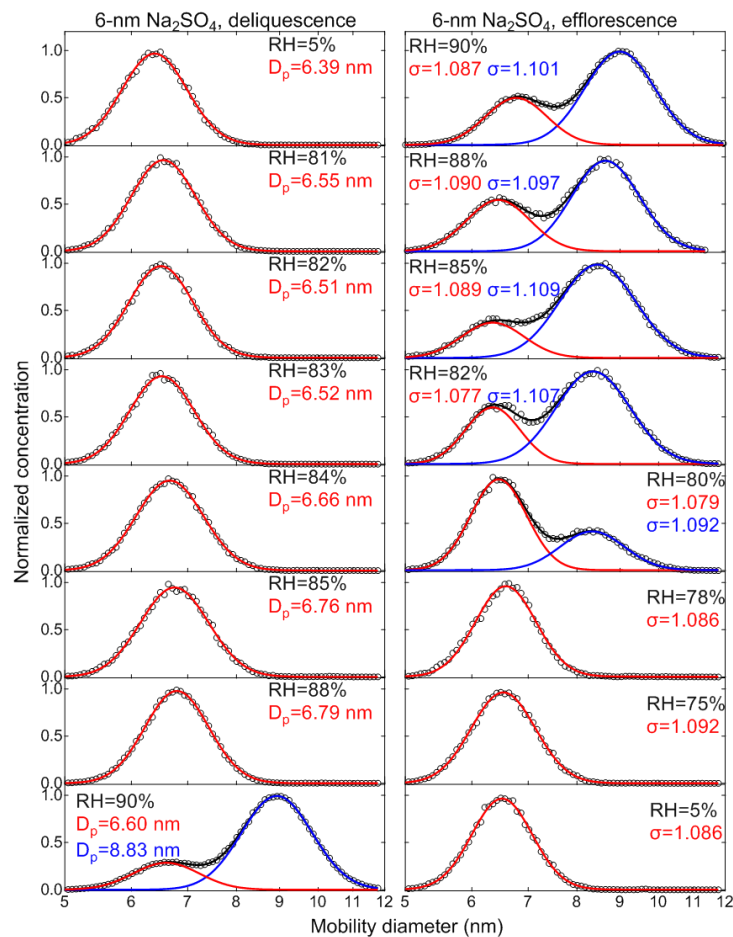
108

109 **Figure S9.** Deliquescence-mode (a) and efflorescence-mode (b) of 20-nm sodium sulfate aerosol nanoparticles. The
 110 measured (black square) and fitted (solid lines) normalized size distribution are shown for increasing RH (5%→X%,
 111 where X is the RH value given in each panel) and decreasing RH (5%→97%→X%, where X is the RH value given in
 112 each panel), respectively. Red/blue solid line is fitted by a single-mode log-normal fit. Red, blue, and black lines are
 113 fitted by a double-mode log-normal fit. The red and blue lines represent the aerosol nanoparticles in the solid and liquid
 114 state, respectively. The voltage applied to the nano-DMA's (0-12500 V) is kept within ±1% around the set value shown
 115 in the voltage meter.

Formatted: Justified, Line spacing: Double

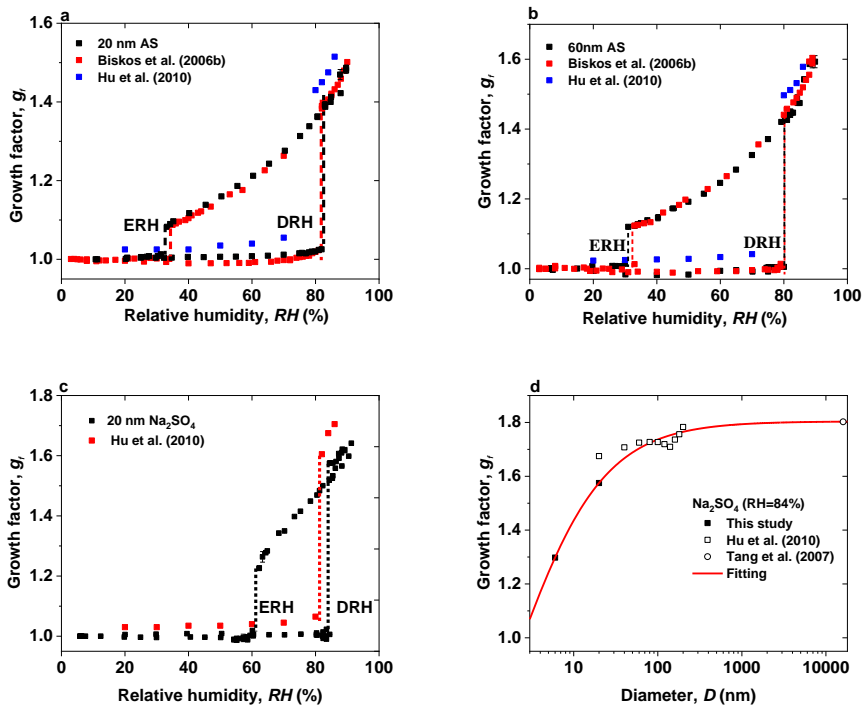
Formatted: Font color: Text 1

Deleted: ¶



117
 118
 119 **Figure S10.** Deliquescence-mode (a) and efflorescence-mode (b) of 6-nm sodium sulfate aerosol nanoparticles. The
 120 measured (black square) and fitted (solid lines) normalized size distribution are shown for increasing RH (5%→X%,
 121 where X is the RH value given in each panel) and decreasing RH (5%→97%→X%, where X is the RH value given in
 122 each panel), respectively. Red/blue solid line is fitted by a single-mode log-normal fit. Red, blue, and black lines are
 123 fitted by a double-mode log-normal fit. The red and blue lines represent the aerosol nanoparticles in the solid and liquid
 124 state, respectively. The voltage applied to the nano-DMAs (0-350 V) is kept within $\pm 1\%$ around the set value shown
 125 in the voltage meter.

Formatted: Font color: Text 1



126

127

128

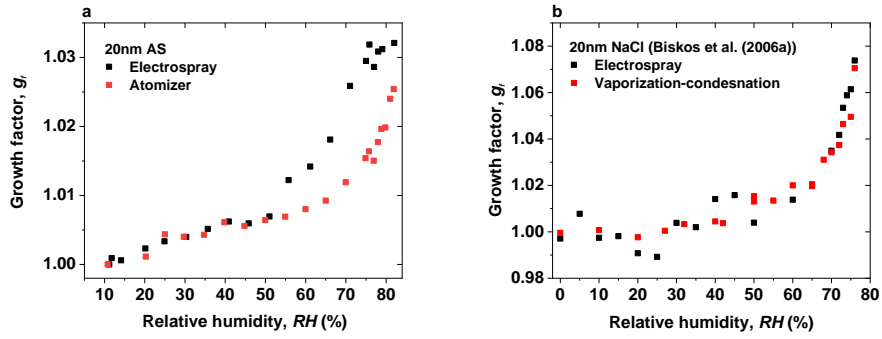
129 **Figure S11.** (a) Comparison of mobility-diameter hygroscopic growth factors (g_f) of 20-nm (a) and 60-nm (b)
 130 ammonium sulfate (AS) nanoparticles with Biskos et al. (2006b) and Hu et al. (2010). (black squares: in this study;
 131 red square: Biskos et al. (2006b); blue square: Hu et al. (2010)). (c) Comparison of mobility-diameter hygroscopic
 132 growth factors of 20-nm Na_2SO_4 nanoparticles with Hu et al. (2010). (black squares: in this study; red square: Hu et
 133 al. (2010)). (d) Mobility-diameter hygroscopic growth factors of Na_2SO_4 nanoparticles with diameter from 6 nm to
 134 14~16 μm at 84% RH (black solid squares: in this study; black open square: Hu et al. (2010); black open cycle: Tang
 135 et al. (2007)). A fitting equation ($g_f = \frac{1.804}{1+(0.5267 \cdot D)^{-0.8194}}$) based on this study at 6-nm, 20-nm Na_2SO_4 , and 14~16 μm
 136 data from Tang et al. (2007).

137

138

139

140



141

142 **Figure S12.** Hygroscopic growth factors of 20-nm (a) ammonium sulfate (AS) nanoparticles from our study and (b)
 143 sodium chloride (NaCl) nanoparticles from Biskos et al. (2006a) using the different generation methods prior to
 144 deliquescence of ammonium sulfate.

145

146

147

148

149

150

151

152

153

154

155

156

157

158

159

160

161

Field Code Changed

Field Code Changed

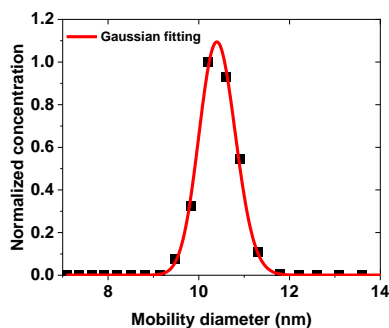
Formatted: Font color: Text 1

162 **S1. Calculation of sizing offset of 10-nm AS**

163 The mobility growth factor (g_f) is given by:

164
$$g_f = \frac{D_m(RH)}{D_m(<10\% RH)}$$
 (S1)

165 g_f was from the data of Biskos et al. (2006b) in the different RHs (see the SI. Fig.5). D_m was
166 retrieved the data of Biskos et al. (2006b) in the different RHs (see the SI. Fig.2) as follows:



167 **Figure S1.3.** Measured (black square) and fitted (red solid line) normalized number size distributions are show for
168 ammonium sulfate aerosol particles at 25% RH. The black square symbols show the data of Biskos et al. (2006b) (see
169 the S1. Fig. 2).

171 Therefore, the initial dry mobility diameter ($D_m (< 5\% RH)$) was obtained using Eq. (S1) based on
172 values of g_f and D_m in the different RHs (see SI. Table S4). We further calculated the average sizing
173 offset of 10-nm ammonium sulfate of Biskos et al. (2006b) system based on the values of $D_m (<$
174 $5\% RH)$. The average sizing offset of 10-nm was ~3.1%.

Deleted: ¶

Formatted: Left

Deleted: 2

Deleted: Table S4. The values of D_m , g_f , and $D_m (< 5\% RH)$ of 10-nm ammonium sulfate of Biskos et al. (2006b) system in the different RHs.¶

Formatted: Left, Line spacing: Multiple 1,08 li

S2. Calculation of sizing accuracy of sub-100 nanoparticles

Knutson and Whitby (1975) proposed the following theoretical differential mobility analyzer (DMA) transfer function and showed that sizing is crucially depend on sheath flow rates and high voltage (HV) applied to the DMA.

$$z_p^* = \frac{Q_{sh} \ln \frac{r_2}{r_1}}{2\pi LV} \quad (S2)$$

$$z_p^* = \frac{neC_c}{3\pi\mu d_p^*} \quad (S3)$$

$$d_p^* = \frac{2VLneC_c}{3\mu Q_{sh} \ln \frac{r_2}{r_1}} \quad (S4)$$

where z_p^* is the central electrical mobility, Q_{sh} is the sheath flow rate, V is the applied voltage, L is the length of the classification region within the DMA, and r_1 and r_2 are the inner and outer radii of the DMA annulus, respectively. n is the number of elementary charges of particles, e is the elementary charges, C_c is the slip correction, μ is the flow viscosity, d_p^* is the mean particle mobility diameter.

According to Eq. (S4) above, we use the following error propagation formula ((Taylor and Taylor, 1997) to calculate the uncertainties in sizing of nanoparticles. In our study, the flow accuracy of mass flow meter (TSI series 4000) is within $\pm 2\%$. The deviation of voltage applied to the nano-DMAs (0-12500 V, 0-350 V) varies around the set value when test with voltage power supply (HCE 0-12500, HCE 0-350, Fug Electronic) shown in Table S5. Thence, the uncertainties in sizing of nanoparticles are obtained based on the following Eq. (S5) as shown in Table S5.

$$\frac{\delta d}{d} = \sqrt{\left(\frac{\delta V}{V}\right)^2 + \left(\frac{\delta Q_{sh}}{Q_{sh}}\right)^2} \quad (S5)$$

Formatted: Font color: Text 1

Formatted: Left, Line spacing: Multiple 1,08 li